Department of Precision and Microsystems Engineering

Improving the noise robustness of reset controllers using an observer

Tiis van der Werf

Report no : 2022.025
Coach : Nima Karbasizadeh
Professor : S. Hassan HosseinNia
Specialisation : Mechatronic System Design
Type of report : Master thesis
Date : 27 June 2022

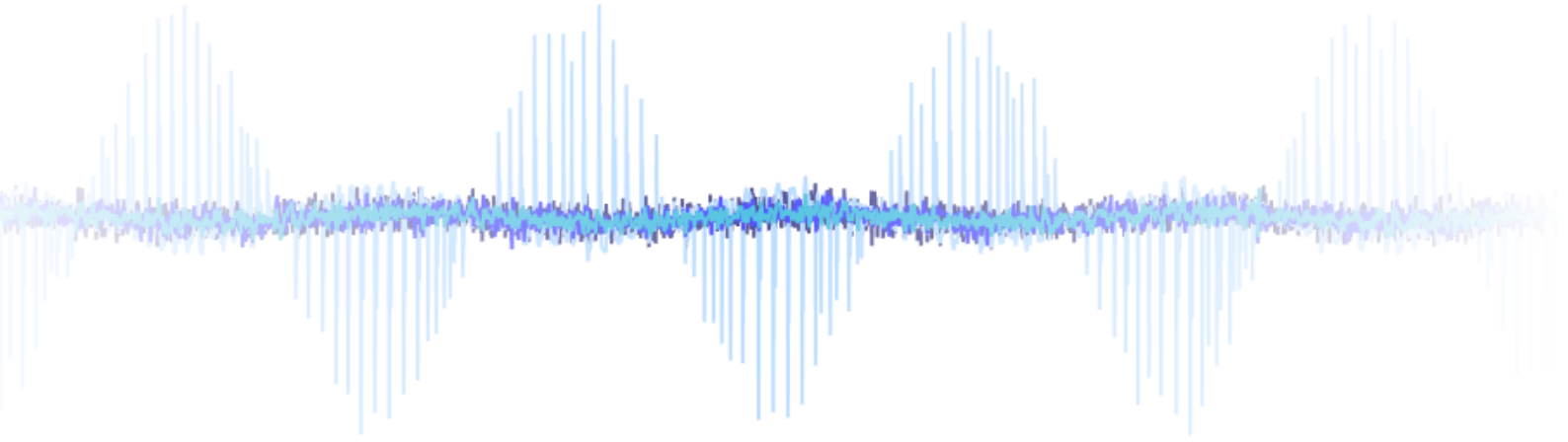

Improving the noise robustness of reset controllers using an observer

by

T. van der Werf

to obtain the degree of Master of Science
at the Delft University of Technology
to be defended publicly on Monday July 11, 2022 at 12:30.

Student number:	4602498	
Project duration:	September 1, 2021 – June 27, 2022	
Thesis committee:	Dr. ir. S. Hassan HosseinNia,	TU Delft, supervisor
	Ir. Nima Karbasizadeh,	TU Delft, daily supervisor
	Ir. Arnold Zondervan,	Hittech Multin
	Dr. ir. Dimitris Boskos,	TU Delft

TU Delft

Abstract

The performance of linear control is limited by the waterbed effect, while the performance demands of industry are continuously increasing. Using non-linear control in the future is therefore unavoidable. Being non-linear, reset control is able to achieve better performance than linear control. However, the lack of robustness to measurement noise withholds most reset controllers from being implementable in industry. The high frequency content of the noisy measurement signal causes excessive resets, which degrade the reset controller performance. In this thesis, two control loop architectures are studied while using an observer to filter out the measurement noise. Prior research is exploited to derive stability conditions and the performance of the two loop architectures is analyzed. The results show that the tracking performance of a CgLp-PID and CR-CgLp-PID controller with noisy measurements is improved by reducing the pseudo-sensitivity over a broad frequency range. The overshoot in the transient response is removed and the performance is not influenced by modelling inaccuracies in the observer when reset feedback line filtering is used. The presented architectures thus improve the reset control systems, making them well implementable in practical setups.

T. van der Werf
Delft, July 1, 2022

Contents

1 Introduction

1.1. Introduction

Accurate motion control is deeply embedded in semiconductor production, (medical) imaging, and data storage. Extensive research has been done into the methods to actuate motion systems to an high level of precision at very high speeds. The high tech industry is continuously improving the performance of their positioning systems, for instance to reduce the chip size. However, most of the improved control techniques developed by research are not yet implemented by industry, because they are often complex and doubts exists about their reliability. Currently, almost all control schemes are completely linear and are based on the PID controller. The accuracy demand will inevitably exceed the limited performance that can be reached by linear control because it is restricted by Bode's gain phase relationship. This relationship implicates that improving high frequency noise attenuation comes at the cost of reducing low frequency disturbance rejection and the other way around, also known as the waterbed effect ([1], p277). This trade-off only applies to linear controllers. In order to improve controllers beyond the waterbed effect to keep meeting market demands, research is done into the possibilities of non-linear control.

Reset control has been studied as a non-linear control method and can be utilized to further improve controller performance without large compromises [2–5]. Multiple contributions have shown the possible performance gain in practice when using reset control. For example, reset control can reduce the overshoot and settling time, while improving disturbance rejection as well [6]. To improve tracking, steady-state precision, and bandwidth frequency, the 'Constant-in-Gain Lead-in-Phase' (CgLp) element can be added to linear controllers for extra phase without the compromise of an increase in gain [7, 8]. Recently, the CgLp element was further improved in overshoot and settling time performance when used in a Continuous Reset (CR) structure [9]. In addition, this structure also provides a continuous controller output which is more feasible for an actuator.

1.2. Problem definition

While quite some research has shown the benefits of reset elements, there are still disadvantages that remain unsolved. A major drawback of some promising reset controllers is the lack of robustness to measurement noise [9]. Lead filters in the controller amplify the high frequency spectrum in the error signal [10]. This causes excessive zero-crossings and thus excessive reset actions, which lead to the performance degradation of those reset controllers. The capacity of modern control systems to perform in non-ideal environments is crucial. Hence, a solution to improve the robustness of reset control to measurement noise is needed.

1.3. Research goal

The goal of this thesis is to provide a solution to the performance degradation of CgLp based reset controllers that is caused by measurement noise. A crucial design requirement is a solution that blends with the conventional control design techniques which are focused on the frequency domain. This implies that the solution should be implementable in state-of-the-art loop shaping methods. Besides

this, the solution should not degrade other aspects of the controller performance, such as the stability margins.

1.4. Thesis Outline

This thesis starts with background information on linear control and observer theory in chapter 2. Next, the preliminaries of reset control are stated in chapter 3, after which the effects of measurement noise on reset control are analyzed in chapter 4. In chapter 5 a control loop is proposed for which a transfer function is derived. The analytical function is validated with simulations that analyze the steady-state and transient performance. After this, in chapter 6 reset feedback line filtering is proposed and analyzed including stability conditions. Chapter 7 concludes the thesis and finally the possible future research directions are discussed in chapter 8.

2

Background information

2.1. Motion control

High-tech machines contain a lot of moving parts that need to be positioned with a certain speed and accuracy. The algorithm that calculates the right actuation forces to move these parts is called the controller. In this section, the basics of controllers are explained using an example. Fig. 2.1a shows a kart that can move horizontally with respect to its base. In order to move the kart, a force $F(t)$ is pushing it. The controller is calculating an optimal force that pushes the kart toward its destination as fast as possible, as precise as possible. The control algorithm is explained by meas of the block diagram in Fig. 2.1b. A desired trajectory, called the reference $r(t)$ is given as input to the system. The kart dynamics are represented by the transfer function $P(s)$, and are often called plant dynamics. The difference between the desired position, the reference, and the actual position $y(t)$, is called the error $e(t) = y(t) - r(t)$. The error is used to calculate the optimal force in the controller, denoted by $C(s)$. This optimal force is called the control output $u(t)$. This control output is converted to a force by an actuator which results into a position change by means of the physical kart. This new position is then fed back in the control loop to calculate the error again.

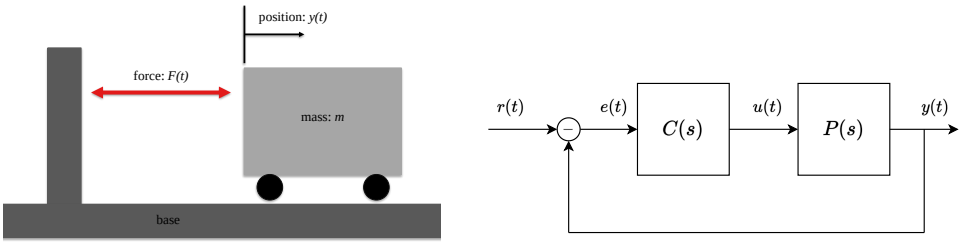

(a) A mass system

(b) A simple control loop

Figure 2.1: Explanatory graphs about the control loop

2.1.1. PID controller

The most commonly used controller is the proportional, integral, derivative (PID) controller. The control output is calculated as follows:

$$u(t) = K_p \left(e(t) + K_i \int_0^t e(\tau)\, d\tau + K_d \frac{de(t)}{dt} \right) \tag{2.1}$$

The the parameters K_p, K_i, K_d can be tuned to get an optimal performance of the controller and tune it for specific plant dynamics. For an analysis in frequency domain, the controller is often described as in (2.2).

$$PID(s) = P \cdot (1 + \frac{\omega_i}{s}) \cdot \frac{s}{\omega_d} + 1 \tag{2.2}$$

2.1.2. Pseudo-sensitivity

The sensitivity represents the ability of the control loop to suppress disturbances that act on the system and can be used to benchmark a control loop. A low sensitivity indicates a good suppression. Besides this, the peak in the sensitivity can be related to the phase margin of the closed loop system. The function defined in (2.3) is used to calculate this sensitivity.

$$S = \frac{1}{1 + C(s)P(s)} \tag{2.3}$$

However, this function assumes that the control system is linear. If a sensitivity analysis needs to be done for a control loop which includes a non-linear element, the pseudo-sensitivity is used. It cannot directly be calculated analytically, but requires an approximation using simulation data. The pseudo-sensitivity is defined as the ratio between the absolute maximum steady state error, and the reference amplitude [11].

$$S_\infty(\omega) = \frac{\max\limits_{t>t_{ss}} |e(t)|}{|A_{ref}|} \tag{2.4}$$

2.2. Limitations of linear control

Linear control is inherently limited by linear relations, which poses a design trade-off on its performance. Two frequency domain limitations are discussed here, more fundamental analysis can be found in [12, 13].

2.2.1. Waterbed effect

The (pseudo-)sensitivity graph can be separated in two sections separated by the bandwidth frequency: a low frequency part with values smaller than 0dB and a high frequency part with values larger than 0dB. There is a linear relation between the area below the bandwidth frequency and the area above the bandwidth frequency. This relation is described by the Bode Sensitivity Integral in (2.5) [1].

$$\int_0^\infty \ln |S(\omega)| \, d\omega \tag{2.5}$$

This integral is zero when a linear system is considered and the open-loop transfer function has at least two more poles than zeros. Additionally, all the poles should be located in the left half plane [1]. These conditions imply for all linear, stable systems that are of an order higher than one. The Bode

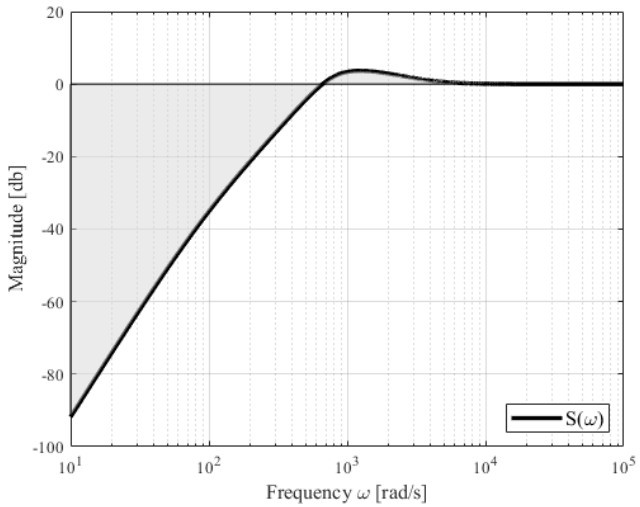

Figure 2.2: The sensitivity function of a mass plant controlled by a CR-CgLp-PID controller. The grey area represents the Bode Sensitivity Integral.

Sensitivity Integral is visualized by the grey area in Fig. 2.2, but since the sensitivity is plotted on

logarithmic scale, their equal size is not well visualized. The integral being zero implicates that the area under the 0dB line and above are of equal size. For linear systems it is not possible to bypass this condition and reducing the sensitivity for low frequencies by choosing different controller parameters would increase the grey area above the bandwidth frequency as well. In other words, the sensitivity for high frequencies is increased in order for (2.5) to remain zero. This trade-off is called the waterbed effect and is a property of linear control. The performance of linear control is therefore limited by the waterbed effect.

2.2.2. Bode's gain phase relationship

The limitations of linear control loops can also be seen in the open-loop bode plot. Bode's gain phase relationship connects the slope of the gain with the phase as in (2.6). A full derivation and more in dept analysis can be found in [13]. The relationship implicates that if one increases the open-loop phase to improve the phase margin, the gain of the system is affected following (2.6). This again limits the performance of linear control, and is one of the main motivations to use non-linear control. It is later shown that reset control is able to break this linear relation.

$$\angle(G(i\omega)) \approx \frac{\pi}{2}\frac{d\log\left|G(i\omega)\right|}{d\log(\omega)} \tag{2.6}$$

2.3. Observer Theory

Disturbance and state observers have been widely used in industry to improve linear system performance [14–16]. Observers were introduced to estimate the states of a process that are not measurable, but are needed for the control algorithm [17, 18]. The Kalman filter (KF) and the Luenberger observer (LO) are examples of such estimators [19–22]. Note the difference between the Luenberger observer and a static Kalman filter, since both state estimators use the exact same architecture and only the correction gain vector is calculated differently. First, the general observer equations are introduced. The state observer is a set of equations that estimates the states of a process. Besides retrieving hidden states, the estimation can also be used to filter a measurement signal which will be utilized in this thesis. A brief explanation which introduces the mathematics of state estimators will follow.

2.3.1. State estimation

Consider a plant process to be estimated by an observer, based on control input u and plant output y_p.

Plant process .
The plant process which is required to be estimated can be modeled as a state space system in (2.7).

$$\begin{aligned} \dot{x}_p &= A_p x_p + B_p u \\ y_p &= C_p x_p + D_p u \end{aligned} \tag{2.7}$$

Estimation .
The observer uses the control output to make an estimation about the state of the plant.

$$\dot{\hat{x}} = A_L \hat{x} + B_L u + w_L \tag{2.8}$$

Where $\hat{x}$ is the preliminary estimation of the true plant state x_p, and w_L is the process noise with $p(w_L) \sim N(0, Q)$, which is assumed to be normally distributed process noise. Note that the actual plant process can differ from the model in the observer. In other words, the state space matrices $\{A_L, B_L, C_L, D_L\}$ are not necessarily equal to $\{A_p, B_p, C_p, D_p\}$.

Sensing .
A sensor measurement z is modelled as:

$$z = C_p x_p + v_m. \tag{2.9}$$

Where v_m is representing the measurement noise, which is assumed to be normally distributed: $p(v_m) \sim N(0, R)$.

Correction .
Using the above, a correction on the state estimation is done based on the observer gain L vector multiplied by the estimation error.

$$\dot{\hat{x}} = A_L\hat{x} + B_L u + L(z - \hat{y}) \tag{2.10}$$

Finally, the observer output is calculated as in (2.11).

$$\hat{y} = C_L\hat{x} + D_L u \tag{2.11}$$

2.3.2. Observer gain vector

In order to improve, rather than degrade the performance when adding an observer to the control loop, close attention should be given to calculation of the observer gain vector. There is a known trade-off, higher observer gain results in faster convergence to real plant states and also means more influence of the measurement noise on the observed states. The problem of choosing L can be cast into a pole placement problem of the observer state transition matrix $(A_L - LC_L)$. If the set (A, C) is observable, there exists a vector L that can map the eigenvalues of the transition matrix everywhere in the complex plain. For stability reasons, these eigenvalues should be in the left half plain and shouldn't coincide with the eigenvalues of matrix A_L.

The calculation of the observer gain can also be cast into a LQR problem that can be solved to obtain the optimal vector. This LQR problem boils down to solving a Riccati equation. The continuous time Riccati function for the observer gain is formulated as (2.12).

$$A_L^T P + PA_L - PC_L^T R^{-1} C_L P + Q = 0 \tag{2.12}$$

If (2.12) is solved for P, the observer gain vector can be calculated by using $L = PC_L R^{-1}$. When measurement and process noise are assumed to be white and time-invariant, the observer is also known as the static Kalman filter. If the covariance terms Q and R are time-variant, the gain is usually calculated real time and then the observer is also known as the general Kalman filter. In this thesis the assumption is made that the noise terms are time-invariant.

The calculation of the observer gain by means of (2.12) is used in this thesis to tune the observer, since it is also the optimal gain vector if model uncertainties do exist. Moreover, if there exists knowledge about the "size" of the uncertainties, this can be incorporated in the Q term of (2.12).

3

Reset control systems

In this section, the basic theory behind reset control is introduced. First, the Describing functions are explained as the general method to describe the non-linear reset systems in frequency domain. Next, the most common reset controllers from literature are stated, after which the stability of reset controllers is discussed.

3.1. Reset control law

Reset control is a non-linear form of control that most commonly relies on a zero-crossing reset law. A general state space form can be written down as a Single Input Single Output (SISO) system as in (3.1). It behaves as a linear system for non-zero input $e(t)$. When the input crosses zero, the state is 'reset' by means of the A_ρ matrix. Generally this matrix has a diagonal shape: $A_\rho = diag(\gamma_1, \gamma_2, ..., \gamma_n)$, with $\gamma \in [-1, 1]$. Different types of reset matrices can be considered as for example non-zero reset values are required to reach steady state targets [23]. Besides this, it was shown that resetting only one term of the A_ρ matrix, called a single state reset, could benefit the tracking performance when higher order reset elements are used [24].

$$(R): \begin{cases} \dot{\mathbf{x}}_r(t) = A_r \mathbf{x}_r(t) + B_r e(t) & \text{if } e(t) \neq 0, \\ \mathbf{x}_r(t^+) = A_\rho \mathbf{x}_r(t) & \text{if } e(t) = 0, \\ u(t) = C_r \mathbf{x}_r(t) + D_r e(t). \end{cases} \tag{3.1}$$

The A_r, B_r, C_r, D_r matrices form the base linear system (BLS). The set of equations can be separated in a flow and a jump set, being the base linear and resetting equation respectively.

3.2. Describing Functions

Non-linear systems are inherently not perfectly described by one frequency domain function. However, a frequency domain function is often required to analyse control systems. A quasi-linearization, called the Describing Function (DF), is used to approximate the frequency response of nonlinear systems ([25], p27). The DF is used for the frequency analysis of reset systems, where sinusoidal inputs are used as excitation for the system. However, the DF method only takes the first harmonic of the Fourier series decomposition while higher-order harmonics are neglected. As will be shown in this thesis, only using the first harmonic can lead to very inaccurate approximations. The Higher Order Sinusoidal Input Describing Function (HOSIDF) is used to calculate the higher-order harmonics of the output signal of non-linear controllers. The HOSIDF method for reset elements defined by (3.1) was introduced by [26] as:

$$H_n(\omega) = \begin{cases} C_r(j\omega I - A_r)^{-1}(I + j\Theta(\omega))B_r + D_r, & n = 1 \\ C_r(j\omega I - A_r)^{-1} j\Theta(\omega) B_r, & \text{odd } n > 2 \\ 0, & \text{even } n \geq 2 \end{cases} \tag{3.2}$$

where $H_n(\omega)$ is the n^{th} harmonic describing function, with:

$$\Theta(\omega) = \frac{-2\omega^2}{\pi}\Delta(\omega)(\Gamma(\omega) - \Lambda^{-1}(\omega)) \tag{3.3}$$

$$\Lambda(\omega) = \omega^2 I + A_r^2 \tag{3.4}$$

$$\Delta(\omega) = I + e^{\frac{\pi}{\omega}A_r} \tag{3.5}$$

$$\Delta_r(\omega) = I + A_\rho e^{\frac{\pi}{\omega}A_r} \tag{3.6}$$

$$\Gamma(\omega) = \Delta_r^{-1}(\omega)A_\rho\Delta(\omega)\Lambda^{-1}(\omega) \tag{3.7}$$

Usually only a first order approximation is taken into account for loop shaping, which means that accurate results are obtained only if the first harmonic is dominant. However, a first order approximation not always gives enough information and Higher Order Sinusoidal Input Describing Functions (HOSIDF) are required. It is shown that tuning works better if higher harmonics are less dominant [27]. This outcome can be understood easily, since the tuning is based on the first harmonic. If the first harmonic approximation matches reality to a better extend, the tuning is done more accurately. It is also possible to include higher-order harmonics for tuning of the controller. Better results at the cost of a more complex tuning method were obtained [28].

3.3. Commonly used elements

Various forms of reset elements can be described by the system in (3.1). The most common forms are addressed in this section.

Clegg integrator .
In 1958, Clegg introduced this new resetting control scheme with the analog circuit in Fig. 3.1a [29]. This Clegg integrator (CI) is an integrating circuit that resets the output to zero when the input signal crosses zero. An output comparison with a linear integrator is given in Fig. 3.1b The main advantage of adding this reset, is that the integrator has $52°$ less phase-lag than a normal integrator. The Clegg integrator can be formed by (3.1) with coefficients:

$$A_r = 0, B_r = 1, A_\rho = 0, C_r = 1, D_r = 0. \tag{3.8}$$

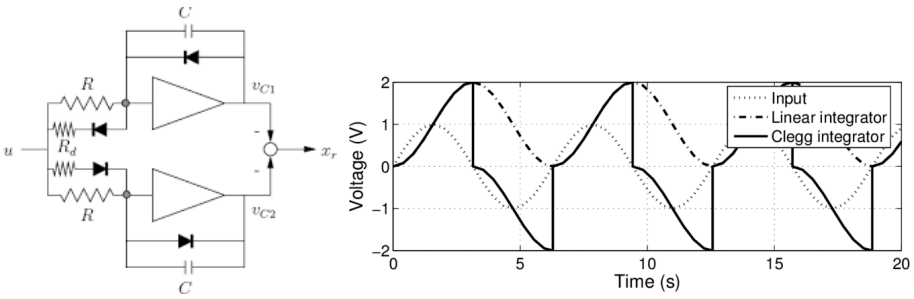

(a) Integrator circuit (b) Input signal and its reset/integrated value

Figure 3.1: Work by Clegg [29]

First Order Reset Element .
The First Order Reset Element (FORE) scheme behaves like a resetting low-pass filter with the same phase advantages as the CI [4]. The FORE can be written as (3.1) with the following coefficients:

$$A_r = -\omega, B_r = \omega, A_\rho = 0, C_r = 1, D_r = 0. \tag{3.9}$$

Second Order Reset Element .
The Second Order Reset Element (SORE) was proposed by [3]. It gives more freedom in the extensions of reset control, since most of the modern PID controllers have additional filtering components

that are of second order. Examples are notch and low-pass filters. While first order elements are often sufficient, a SORE can give more design options with respect to the FORE. They include a damping parameter β which introduces an extra tuning parameter. The SORE is described by (3.1) with:

$$A_r = \begin{bmatrix} 0 & 0 \\ -\omega^2 & -2\omega\beta \end{bmatrix}, B_r = \begin{bmatrix} 0 \\ \omega^2 \end{bmatrix} A_\rho = \mathbf{0}, C_r = \begin{bmatrix} 1 & 0 \end{bmatrix}, D_r = \mathbf{0}. \tag{3.10}$$

PI + CI .
The PI + CI controller consists of one P element and two integrators. When combining a linear and a resetting integrator, one can reduce the limit cycles that occur when only using a resetting integrator and a non-zero force is required at zero error. Another benefit of adding the Clegg integrator to the PI compensator is the transient response of the system as it can reduce overshoot and settling time. Similar behaviour with less overshoot with respect to a PI controller was obtained [30].

Constant gain Lead in phase .
The ”constant-in-gain-lead-in-phase” (CgLp) element was presented as a solution to increase phase without influencing the gain [7]. It is constructed by combining a resetting lag filter $R(s)$, i.e. a FORE or a SORE, with a linear lead filter $L(s)$ in series which are defined in (3.11) and (3.12) respectively. Whereas the previous mentioned elements are mostly used to limit the phase-lag, the CgLp can be used to create phase-lead as can be seen in Fig. 3.2. This figure shows that the CgLp element is able to break the relation in (2.6). The proposed control scheme adds the CgLp block before a PID controller. The phase margin is then retrieved from the CgLp element, and the D action of the linear controller is made minimal to only ensure stability of the BLS. Tuning has been investigated thoroughly, and is still an active subject in research [8,28,31].

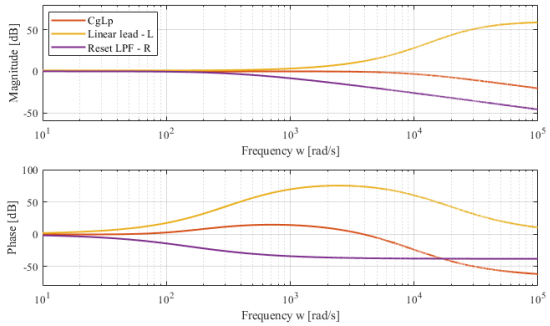

Figure 3.2: Broadband phase lead achieved with CgLp using FORE in the range $[\omega_r = 172, \omega_f = 9420]$ with $\gamma = 0$, and $\omega_{r\alpha} = 0.93\omega_r$

$$R(s) = \frac{1}{s/\omega_{r\alpha} + 1}^{\gamma} \tag{3.11}$$

$$L(s) = \frac{s/\omega_r + 1}{s/\omega_f + 1} \tag{3.12}$$

The state space matrices of the CgLp element are:

$$A_r = \begin{bmatrix} -\omega_{r\alpha} & 0 \\ \omega_f & -\omega_f \end{bmatrix} B_r = \begin{bmatrix} \omega_{r\alpha} \\ 0 \end{bmatrix} A_\rho = \begin{bmatrix} \gamma & 0 \\ 0 & 1 \end{bmatrix}, C_r = \begin{bmatrix} \frac{\omega_f}{\omega_r} & (1 - \frac{\omega_f}{\omega_r}) \end{bmatrix}, D_r = \mathbf{0}. \tag{3.13}$$

Continuous reset architecture .
A different control architecture for reset elements was introduced to create a continuous output signal [9]. The previously mentioned reset elements all create dis-continuous output signal. If such signals are demanded from real actuators, practical problems regarding saturation, rise time, and excitation of higher resonance modes are created. The continuous output from the continuous reset (CR) architecture tackles this problem. Besides this, the architecture also reduces the sensitivity peak when used in combination with a CgLp element. The continuous reset (CR) structure consists of a lead filter, reset element, and a lag filter in series. The lead and lag filters are defined by (3.14).

$$L(s) = \frac{s/\omega_l + 1}{s/\omega_h + 1}, \quad R(s) = \frac{1}{s/\omega_l + 1} \tag{3.14}$$

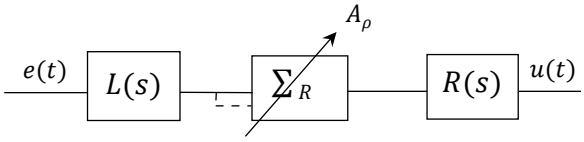

Figure 3.3: Block scheme of the CR structure [9].

If ω_h is chosen to be relatively large enough with respect to the bandwidth frequency, the CR lead and lag filters cancel each other and almost do not influence the DF of the controller. With the same assumption, one can approximate the reset law by

$$e_r(t) = \dot{e}(t)/\omega_l + e(t) = 0. \tag{3.15}$$

It has been shown that the magnitude of higher-order harmonics is reduced by putting a reset element inside the CR structure. As a result, the first-order DF will be a better approximation of the actual controller and the result of the loop-shaping procedure is closer to ideal. It is also shown that the transient response of the controller is improved significantly with this architecture [9].

3.4. Stability of reset control

As with all controllers, stability has to be ensured for reset controllers. It is shown that, under the right conditions, a second order plant that is stabilized by a linear integrator, cannot be stabilized using a Clegg integrator [32]. Moreover, it is shown that a Clegg integrator can stabilize certain second order plants that cannot be stabilized by a linear integrator. Therefore new methods are developed to verify the stability of reset control systems.

Systems with reset elements can roughly be divided into two categories: with a stable or an unstable base linear system. If the BLS is stable, stability can be proven with the H_β condition. It secures quadratic stability and implies Uniform Bounded-Input Bounded State (UBIBS) stability of (3.1). Beker [33] reformulated the H_β condition such that it does not require assumptions about the evolution of reset times. However, if the base system is unstable, other conditions apply [34]. These conditions are reset time dependent, but can be used for systems with unstable base systems as well. In this thesis, the H_β condition for stable BLS is used.

The H_β condition .
When the base linear system (BLS) is stable, the quadratic stability of the closed loop system (3.1) can be examined by the following theorem [9].

Theorem 1. *There exists a constant $\beta \in \mathbb{R}^{n_r x 1}$ and positive definite matrix $P_\rho \in \mathbb{R}^{n_r x n_r}$, such that the restricted Lyapunov equation*:

$$P > 0, \quad A_{cl}^T P + P A_{cl} < 0 \tag{3.16}$$

$$B_0^T P = C_0 \tag{3.17}$$

has a solution for P, where C_0 and B_0 are defined by

$$C_0 = \begin{bmatrix} \beta C_p & 0_{n_r \times n_r} & P_\rho \end{bmatrix}, B_0 = \begin{bmatrix} 0_{n_p \times n_r} \\ 0_{n_{nr} \times n_r} \\ I_{n_r} \end{bmatrix} \tag{3.18}$$

and

$$A_\rho^T P_\rho A_\rho - P_\rho \leq 0 \tag{3.19}$$

where A_{cl} is the closed loop A-matrix. n_r is the number of states being reset and n_{nr} being the number of non-resetting states and n_p is the number of states for the plant. A_p, B_p, C_p, and D_p denote the state space matrices of the plant.

A downside of the presented stability methods above is that they rely on parametric models for the analysis. To tackle this problem, different a different method based on frequency response function (FRF) data was presented [35]. This work was extended for systems that reset to non-zero values and/or have shaping filters [36]. Using these methods, the stability can directly be determined from FRF measurements of the base linear open-loop system.

4

Reset control and noise

This chapter analyses the performance degradation of reset controllers due to the measurement noise. All sensors introduce noise and it is inherent to practical implementations. The ability of the reset controller to be robust to measurement noise is therefore critical. Measurement noise is not beneficial for the performance of all controllers because they are relying on the correctness of the error data that is based on the measurement data. To quantify the measurement noise, a Signal-to-Noise-Ratio (SNR) is defined by (4.1).

$$SNR = \frac{1}{k}\sum \frac{P_{s,rms}(k)}{P_{n,rms}(k)} \tag{4.1}$$

Furthermore, performance degradation due to measurement noise is not specific for reset control as the conventional linear controllers suffer from the same problem [37]. However, when linear control is compared with non-linear control in its robustness to measurement noise, differences are seen. Consider a control loop to be simulated in which a controller is used to act on a first order plant, while white noise is added to the measurements. In Fig. 4.1, the pseudo-sensitivity for noisy and clean measurements on different controllers is shown. It visualizes the minimum error that is introduced by the noise. For linear control this is predictable by using (2.4) and for this specific example the minimum is calculated in (4.2). The minimum is equals the SNR for the linear PID controller. It is observed that the non-linear reset controllers indeed suffer more from measurement noise than the linear PID controller.

$$S_\infty(\omega = 0) = \frac{\sqrt{R_n f_s}}{A_{ref}} = -46.5\ dB \tag{4.2}$$

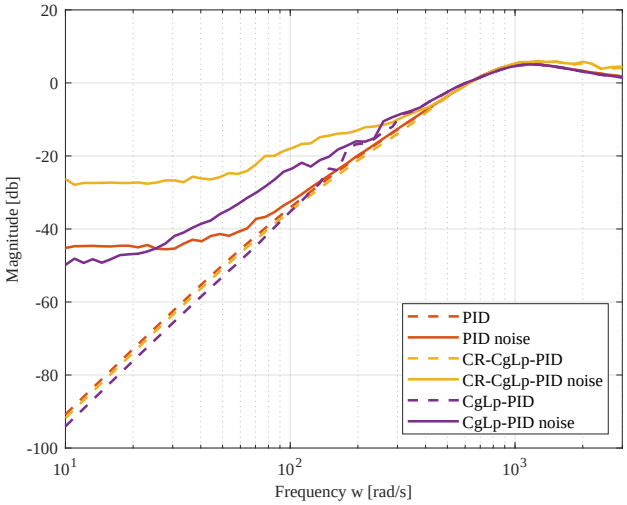

Figure 4.1: Pseudo sensitivity of linear and non-linear controller with and without white noise, $P_n = 2e^{-12}$W

Moreover, the excessive resets resulting from the noise are visualized in Fig. 4.2. For the control loops without noise, periodic resets are seen whereas for the loops with noise, the reset condition is triggered excessively. The difference between the CR-CgLp-PID and CgLp-PID can also be observed. The extra lead filter in the CR structure is amplifying high frequencies of the noise, causing even more resets than the CgLp-PID controller.

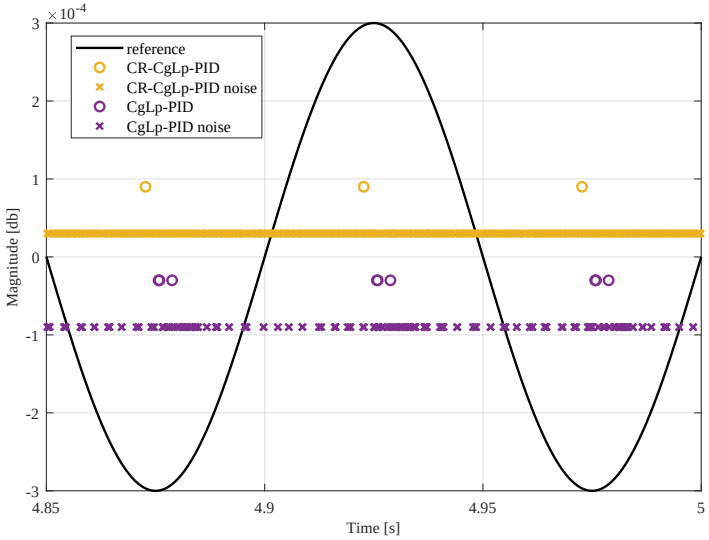

Figure 4.2: Reset instances with and without white noise, $P_n = 2e^{-12}$W, $A_{ref} = 300\mu$m, $f_{ref} = 10$Hz

It can already be seen in Fig. 4.1, but is made more distinct in Fig. 4.3 which shows the difference in the ratio between the noise system and the ideal system for all three controllers. This ratio is described by $S^n - S$. Where the superscript n denotes a noisy measurement.

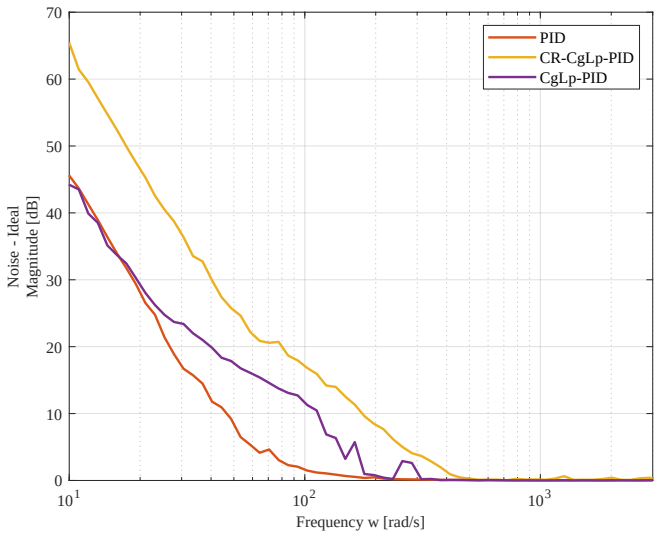

Figure 4.3: Difference in pseudo-sensitivity for linear and non-linear controllers between ideal and noisy measurements, additive white noise $P_n = 2e^{-12}$W

For frequencies up to 500rad/s the deterioration of the CR controller is larger than that of the linear controller. For CgLp controller the increase in deterioration is only seen between 25 and 300rad/s.

Frequency filters such as low pass filters (LPF) have been suggested as a noise filter for reset control [9]. In [10] LPFs are used in the reset line to reduce the excessive zero-crossings. Although the high frequency noise is successfully reduced, a side effect is that the describing function (DF)

gain and phase of the system are negatively influenced. As a result, an increase in the peak of the pseudo-sensitivity is created.

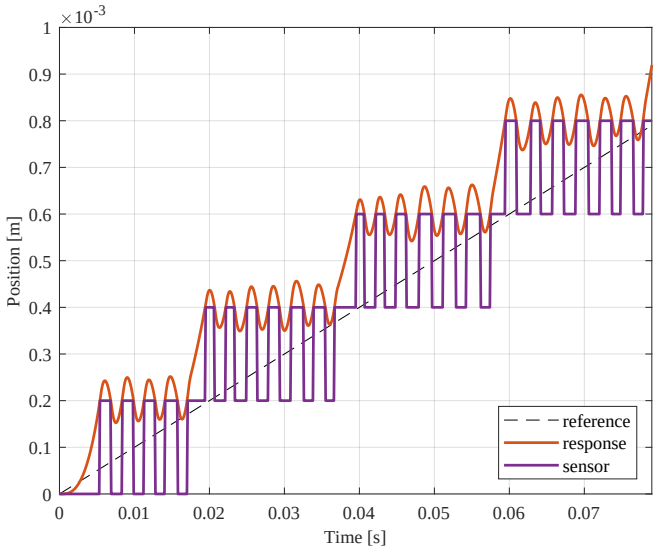

Figure 4.4: Limit cycles induced by the magnitude discretization, $\Delta = 0.2mm$

4.1. Quantization induced degradation

Quantization introduces a specific form of measurement noise and has been studied separately. It is sometimes modelled as white noise, but its stochastic properties are not conform white noise since quantization is bounded and its frequency is dependent on the frequency of the input signal [38, 39]. Quantization has a negative effect on the controller performance when the desired accuracy is in the order of the quantization level. This is caused by the fact that the controller is acting on a quantized sensor signal, which is not equal to the true value. A specific example is the limit cycles that occur as the controller acts on the quantized sensor measurements. The response of a CR-CgLp controller can be seen in Fig. 4.4.

Quantization introduces a so called (error) band on the reset condition. This implies that the reset condition can be met between 0 and Δ if truncating quantization is considered. This band gets even larger if other types of noise are also present. As a result, false resets occur when the error is passing through one of the band limits, but not actually crossing zero. Limiting the maximum resetting frequency has been studied as a method to reduce excessive resets. This is called time regularization of the reset condition and was specifically tested for quantization noise [39]. However, it was shown that the sinusoidal tracking was only improved for a certain frequency band.

That concludes the problem statement. Reset control suffers from measurement noise and is therefore not yet able to reach its full potential in practical setups. There is a need for a broad band noise reduction method that does not influence the DF of the reset controller and is analyzable in frequency domain. This thesis aims for a solution to the lack of robustness to measurement noise of reset controllers.

5

Feedback line filtering

In order to reduce the negative effects of measurement noise, multiple filter locations were investigated during this thesis. An overview of the locations can be seen in Fig. 5.1. The conclusion was drawn that frequency based filters decrease the phase margin of the control loop at all locations. As a result, the extra phase that is gained by using a reset controller, is vanished by its need for a noise filter. Research in observers gave promising results and therefore this section focuses on the possible performance gain when using an observer on location C_1. Stability conditions for this control loop architecture are derived in section 6.

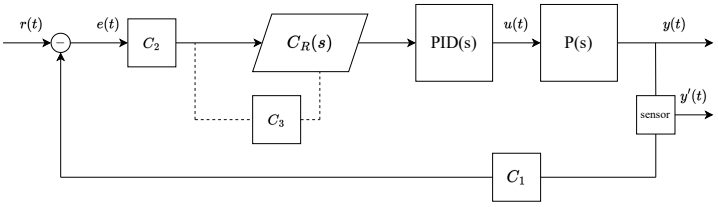

Figure 5.1: Block scheme of a feedback system with filter locations C_1, C_2, C_3

First, an analytical approach is presented which derives a transfer function for the control loop with an observer on the feedback line. Next, simulations are done for two controller types: CgLp-PID and CR-CgLp-PID. For each controller, two cases are considered. The first case studies measurement noise, and the second case is done to study the robustness to parameter uncertainty as this is the main concern of observer based control. More details regarding the simulation settings can be found in Appendix A.

5.1. Analytical transfer function

An analytical approach to obtain a frequency domain transfer function of the complete system with observer is given in this section. The overall closed loop system visualized in Fig. 5.2, is describe by (5.1). The matrix details can be found in Appendix B.

$$\begin{cases} \dot{\mathbf{x}}(t) = \bar{A}\mathbf{x}(t) + \bar{B}w(t) & \text{if } e_r(t) \neq 0, \\ \mathbf{x}(t^+) = \bar{A}_\rho \mathbf{x}(t) & \text{if } e_r(t) = 0, \\ y(t) = \bar{C}\mathbf{x}(t) & \\ e_r(t) = \bar{C}_e\mathbf{x}(t) + \bar{D}_e w(t) & \end{cases} \tag{5.1}$$

The transfer function is used to approximate the pseudo-sensitivity which is generally obtained by simulations. Next, the derivation of the analytical function for the pseudo-sensitivity is given. A continuous time case is taken as it simplifies the equations with respect to the discrete time case without loss of generality. For details on the discrete time case, the interested reader is referred to Appendix C.

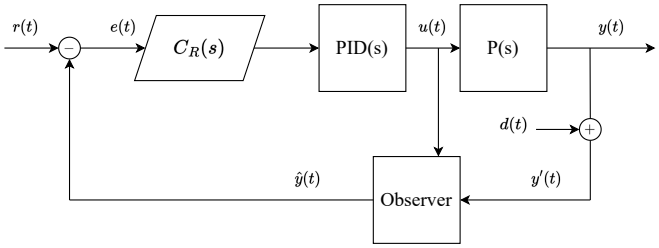

Figure 5.2: Control loop with controller, plant, sensor noise, and the observer on the feedback line.

A linear plant can be represented in state space matrices, and its transfer function for $u(t)$ to $y(t)$ is:

$$P(s) = \frac{Y(s)}{U(s)} = C_p(sI - A_p)B_p. \tag{5.2}$$

Where the subscript p stands for the true plant matrices which are unknown to the controller. The observer equations in time domain are represented by (2.10) and (2.11), which are repeated in (5.3) and (5.4) for convenience.

$$\dot{\hat{x}} = A_L\hat{x} + B_L u + L(y' - \hat{y}) \tag{5.3}$$

$$\hat{y} = C_L\hat{x} + D_L u \tag{5.4}$$

Next, a transfer function is obtained for $u(t)$ to $\hat{y}(t)$. Let the above equations be represented in Laplace domain by:

$$s\hat{X}(s) = A_L\hat{X}(s) + B_L U(s) + LY'(s) - LC_L\hat{X}(s) - LD_L U(s). \tag{5.5}$$

When using $y'(t) = y(t) + d(t)$ in (5.5), where $d(t)$ is the noise function. This function is also rewritten to Laplace domain.

$$Y'(s) = Y(s) + D(s) \tag{5.6}$$

$$s\hat{X}(s) = A_L\hat{X}(s) + B_L U(s) + L(Y(s) + D(s)) - LC_L\hat{X}(s) - LD_L U(s) \tag{5.7}$$

Next, substituting (5.2) in (5.7) gives:

$$\hat{Y}(s) = C_L(sI - A_L + LC_L)^{-1}[(B_L - LD_L + LP(s))U(s) + LD(s)] \tag{5.8}$$

Which can not be written in a one-to-one transfer function from $U(s)$ to $\hat{Y}(s)$, unless the noise function is assumed to be zero. For simplicity, the equation above is rewritten to (5.9)

$$\hat{Y}(s) = Z(s)U(s) + \Delta Z(s)D(s) \tag{5.9}$$

Where

$$Z(s) = C_L(sI - A_L + LC_L)^{-1}(B_L - LD_L + LP(s)), \tag{5.10}$$

and where

$$\Delta Z(s) = C_L(sI - A_L + LC_L)^{-1}L. \tag{5.11}$$

Error and true error .
We implement (5.8) in the equation for the error to come to (5.12).

$$e = r - Z(s)U(s) - \Delta Z(s)D(s) = r - Z(s)C(s)e - \Delta Z(s)D(s) \tag{5.12}$$

Which can be rewritten to get a full equation for the error that is fed to the controller.

$$e = \frac{r - \Delta Z(s)D(s)}{1 + Z(s)C(s)} \tag{5.13}$$

However, this is not the true error, since it is based on the estimation $\hat{y}$ of the observer. Instead, the real error is described by $e_{true} = r - y$. When substituting the plant and controller transfer function, one derives:

$$e_{true} = r - P(s)C(s)e \tag{5.14}$$

Next, the previously derived equation for the error can be substituted to end up with (5.15).

$$e_{true} = r\left[1 - \frac{P(s)C(s)(1 - \frac{\Delta Z(s)D(s)}{r})}{1 + Z(s)C(s)}\right] \tag{5.15}$$

Pseudo-sensitivity .
Next, (5.15) can be used for calculating the pseudo-sensitivity analytically by using $S_\infty(\omega) = \frac{|e_{true}|}{r}$. However, there exist a discrepancy between the maximum absolute steady state error in (2.4), and the Laplace domain formula derived above. The evaluation of the term $\Delta Z(s)D(s)$ in (5.15), should therefore not be at s. The correct evaluation is obtained when the cumulative over all frequencies is taken. For example, when a sinusoidal noise is used, $\Delta Z(s)$ can be evaluated at the noise frequency only since that is the only frequency that gives a non-zero value. Alternatively, if white noise is considered, the cumulative value can be obtained by summing the response over all frequencies. However, this formula remains a linear approximation and will only serve as a guideline.

It can also be seen from this formula that if noise power is zero, and the observer model is matching the plant perfectly, the sensitivity equation reduces to the well known equation $S(s) = \frac{1}{1+C(s)P(s)}$, since in that case $Z(s) = P(s)$ for $\forall L$, and $D(s) = 0$.

5.2. CgLp-PID + observer

In this section, simulations are used to validate the proposed control loop from Fig. 5.2, when using a CgLp-PID controller. It is shown that calculation of the pseudo-sensitivity using (5.15) is an appropriate method to approximate the true pseudo-sensitivity. The first case considers a situation in which the observer has a perfect model of the plant, but it includes measurements which are disturbed by noise. The second case considers a situation in which the measurements are perfect, but the model of the plant is not perfectly matched with the true plant dynamics.

5.2.1. Measurement noise

Consider the closed loop system as shown in Fig. 5.2 including sensor noise with a mass plant that is described by (5.16). The assumption was made that the state space model parameters in the observer are equal to $\{A_p, B_p, C_p, D_p\}$.

$$P(s) = \frac{1}{s^2} \tag{5.16}$$

The sensor noise is modelled as additive white noise, with $P_n = 2e^{-12}$W. Consider the plant to be controlled by a CgLp-PID controller which is tuned at 150Hz bandwidth. Assume the observer to be on the feedback line and defined by (2.10) and (2.11). An observer gain of $L = [0, 0.5]^T$ was used as an example.

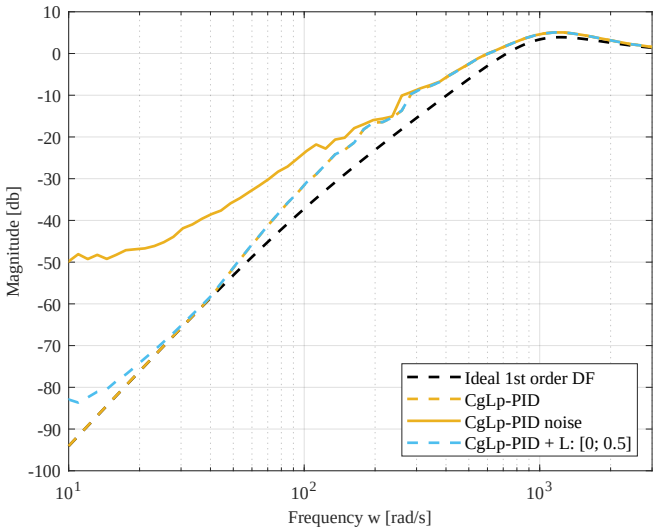

Figure 5.3: Pseudo-sensitivity of mass system controlled by a CgLp-PID controller with and without using an observer.

When the correct model of the plant is given to the observer, tracking can be improved tremendously, as can be seen in the pseudo-sensitivity in Fig. 5.3. The observer is used to filter the noise, and the minimum in the pseudo-sensitivity is reduced at low frequencies.

Since the model in the observer is perfectly describing the plant process, the pseudo-sensitivity can be reduced even further towards the ideal curve for lower frequencies by lowering the observer gain vector to zero. The discrepancy between the DF and the simulations is explained by the fact that the DF only takes the first harmonic into account, whereas the pseudo-sensitivity is including all harmonics which contribute to a larger steady-state error.

5.2.2. Model inaccuracies

In a practical setup, model inaccuracies are introduced since the true plant dynamics are not known to the controller. Studying the observer without considering a non-ideal case may therefore differ a lot from a real situation. This case considers an observer with matrices that do not match the true plant state space matrices. The noise term is kept zero, in order to isolate the change in pseudo-sensitivity due to the model inaccuracy. The model inaccuracy is described by delta-matrices as in (5.17).

$$\dot{\hat{x}}(t) = (A_p + \Delta A)\hat{x}(t) + (B_p + \Delta B)u(t), \hat{y}(t) = (C_p + \Delta C)\hat{x}(t) \tag{5.17}$$

In this simulation, the mass has been increased by 3%. As a result, an increase in pseudo-sensitivity can be seen at lower frequencies in Fig. 5.4. This is explained by the mismatch between the true and observer model. The minimum can be approximated using the same limit of (2.4), which is done in (5.18). Besides this, a similar discrepancy between the numerical and analytical work is seen in the mid range frequency due to the first order approximation.

$$\lim_{s\to 0} \frac{|e_{true}|}{A_{ref}} = \frac{\left|\frac{1+Z(s)C(s)-P(s)C(s)}{1+Z(s)C(s)}\right|}{A_{ref}} = -30.72dB. \tag{5.18}$$

This minimum is undesirable and therefore it is concluded that the performance of the observer is heavily depending on accuracy of the approximation of the plant model. In short, the minimum that is caused by the unavoidable modelling errors should at least be less than the minimum that is caused by the noise. Note that the minimum caused by noise is dependent of A_{ref} and becomes relatively small when the reference amplitude is increased. However, minimum caused by the model inaccuracy will be equal for all reference amplitudes.

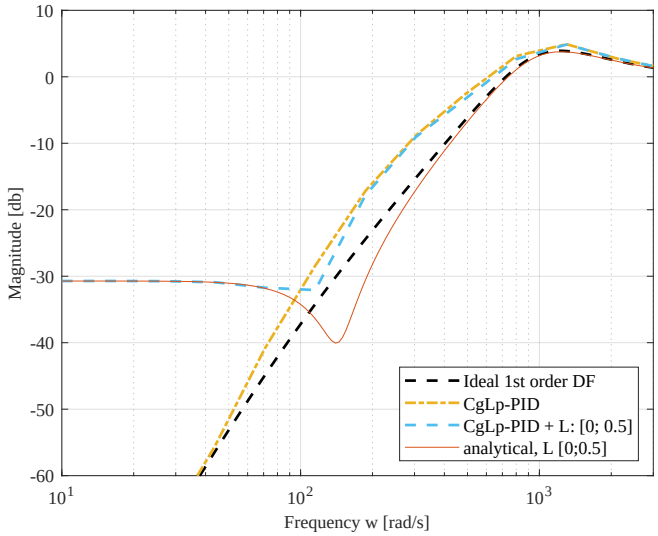

Figure 5.4: Pseudo-sensitivity of mass system controlled by CgLp-PID controller with an observer, analytical and numerical results, with $m_p = 1.03 * m_L$

5.3. CR-CgLp-PID + observer

In this section, the same analysis as in the previous section is done for the system in Fig. 5.2 using a CR-CgLp-PID controller.

5.3.1. Measurement noise

Consider the closed loop system including sensor noise and a mass plant that is described by (5.16). The assumption was made that the state space model parameters in the observer are equal to the plant process matrices. The sensor noise is modelled as additive white noise and the plant to is controlled by a CR-CgLp-PID controller that is tuned on 150Hz. Assume the observer to be on the feedback line and defined by (2.10) and (2.11). The observer gain was set to $L = [0, 0.5]^T$ again for example purposes. Similar to the controller without continuous reset structure, the sinusoidal tracking can be improved as

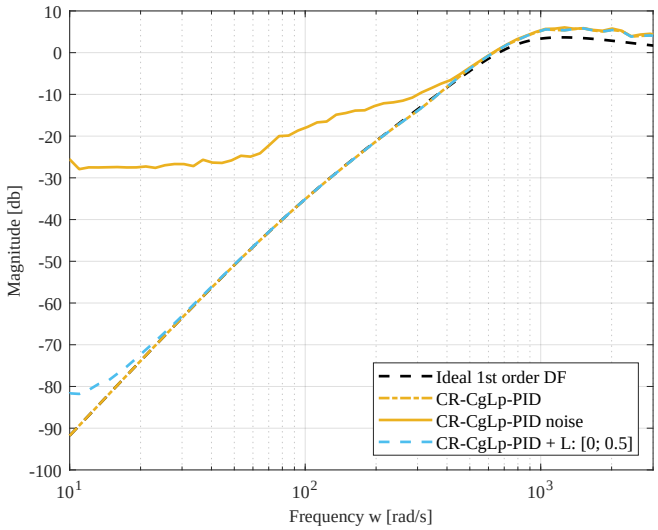

Figure 5.5: Pseudo-sensitivity of mass system controlled with CR-CgLp-PID with and without using an observer, with $P_n = 2e^{-12}$W

is seen in Fig. 5.5. Besides this, less difference is seen between the DF and the pseudo-sensitivity in the mid-range frequencies. This can be explained by the fact that the CR structure reduces the magnitude of the higher-order harmonics of the reset element which increases the accuracy of the first order approximation [9].

Furthermore, a difference is seen in the high frequency spectrum. The convergence to 0dB is not very smooth anymore. This can be explained by the fact that the reference sine is not very smooth at those frequencies, since the data points per period is limited by f_s/f_{ref}. Despite that these frequencies remain below the Nyquist frequency of $f_s/2$, the amplitude is not completely captured anymore and the wave is not smooth. Moreover, these signal will hold more high frequency content. This causes the worse performance the CR-CgLp-PID controller at those frequencies. Since the CR structure adds a lead filter in front of the CgLp element, it is less robust to these high frequencies. Data above $3k$rad/s is not very reliable with the sampling frequency of $10k$Hz. This is a trade-off between simulation speed and maximum reliable frequency.

5.3.2. Model inaccuracies

For the CR-CgLp-PID controller loop, an analysis for model inaccuracies was done. Fig. 5.6 shows the pseudo-sensitivity for $m_p = 1.03m_L$. The analytical results match very well with the simulations, which is remarkable when comparing with the CgLp-PID controller result in Fig. 5.4. This is again explained by the fact that the CR structure decreases the magnitude of the higher-order harmonics of the reset controller. The linear transfer function in (5.15) is therefore a better representation of the actual system. Logically, the robustness to parameter uncertainty remains for CR based reset control when the observer is used on the reset line.

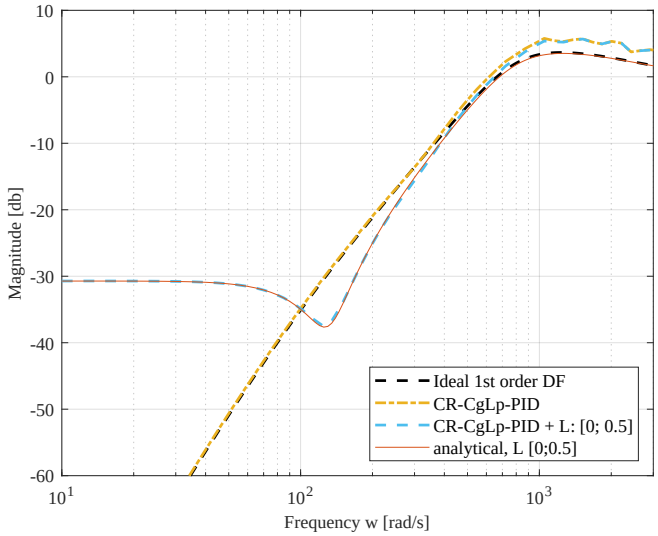

Figure 5.6: Pseudo-sensitivity of mass system controlled with CR-CgLp-PID with an observer, analytical and numerical results, $m_p = 1.03 * m_L$

5.4. Conclusion

An analysis was done on the use of an observer on the feedback line of a reset control loop. A CgLp-PID as well as a CR-CgLp-PID were considered. The transfer function that was derived at the beginning of this chapter was backed by the simulation results when noise is assumed to be zero. However, the effect of higher-order harmonics was visible in the CgLp-PID controller which resulted in a difference between the analytical work and the simulations. This discrepancy was not seen when a CR-CgLp-PID controller is used.

Furthermore, the results show a large reduction in the pseudo-sensitivity when a perfect model of the plant is available in the observer. The pseudo-sensitivity could even be reduced to the ideal curve. However, if model inaccuracies were included in the simulation, the results were less positive. An minimum in sensitivity is seen when the mass was mismatched by 3%. This minimum was predicted by the analytical work, and causes a severe increase the pseudo-sensitivity. It can therefore be concluded that the observer on the feedback line is not favorable for implementation in an experimental setup. Only if a (near-)perfect model is available, and the parameter uncertainty is normally distributed around zero, it would lead to a performance improvement.

6

Reset line filtering

Reset line filtering can improve the reset instances, which was the main motivation of this thesis. The major drawback of general feedback line filtering has shown to be the robustness to parameter uncertainty, therefore research was done in possibilities to improve reset control performance with observers while retaining its original robustness to plant parameter uncertainty. A more focused approach is now considered by only filtering the reset feedback line with the aim to remove the excessive resets, while not changing the original feedback line to the error input of the controller.

In the following paper, a control loop with a separate feedback line for the calculation of the reset condition is proposed. An observer filters the noise out of the measurements and successfully reduces the amount of excessive resets. A second order system was used for the simulations and the architecture was tested on a fourth order practical setup. The new architecture is specifically tested in combination with the CR-CgLp-PID controller, since it suffers most from the measurement noise. The results show a reduction of the pseudo-sensitivity when the SNR is roughly below $50dB$, meanwhile the robustness problem introduced before was not observed.

The paper on the following pages is part of the process of submitting a paper covering the reset line filtering to the Journal of Mechatronics. This journal requires a paper that not only has a theoretical approach, but also includes validation of the work through experiments. At the moment of writing this thesis, the experiments were still ongoing and therefore paper was not yet submitted. Despite the fact that the experimental validation is not complete, first results were backing the numerical simulation results above and those in the paper.

Improving the noise robustness of reset control using an observer

Tiis van der Werf[a], Nima Karbasizadeh[a], S. Hassan HosseinNia[a]

[a]*Department of Precision and Microsystem Engineering, Delft University of Technology, Mekelweg 2, Delft, 2628 CD, The Netherlands*

Abstract

Reset control is able to achieve better performance than linear control. However, the lack of robustness to measurement noise withholds recently designed reset elements from being implementable in industry. The measurement noise present in the reset line creates excessive resets, which degrade the transient and steady-state reset controller performance. This paper presents a new control loop architecture that improves the robustness to measurement noise of reset controllers. The proposed architecture consists of a separate feedback line for the reset condition, which is filtered by an observer. It is shown both theoretically and practically that the new architecture significantly improved the performance with respect to the conventional reset controllers. The transient and steady-state performance of a CR-CgLp-PID controller including measurement noise is improved, while preserving the robustness to parameter uncertainty. Stability conditions for the closed-loop based on the H_β-condition are given and simulation results are verified on an experimental setup.

Keywords: reset control, precision motion control, observer

1. Introduction

The high tech sector is continuously improving the performance of their positioning systems. Currently, almost all control schemes are linear PID controllers with one or two additional linear filters. However, the desired performance is exceeding the performance that can be reached by linear control. More specifically, Bode's integral theorem limits these controllers as it creates a trade-off between disturbance rejection and noise attenuation on one hand, and robustness and transient response on the other hand. This concept is also known as the waterbed effect [1]. This trade-off only applies to linear controllers, and therefore non-linear control does not suffer from the waterbed effect. Consequently, non-linear control can improve upon classical PID control.

Reset control has been studied as a non-linear control method and can be utilized to further improve controller performance without large compromises [2, 3]. For example, reset control can reduce the overshoot and settling time, while also improving disturbance rejection [4]. To improve tracking, steady-state precision, and bandwidth frequency, the 'Constant-in-Gain Lead-in-Phase' (CgLp) element can be added to linear controllers for extra phase without the compromise of an increase in gain [5, 6]. Recently, the CgLp element was further improved in overshoot and settling time performance when used in a Continuous Reset (CR) structure [7]. In addition, this structure also provides a continuous controller output which is more feasible for an actuator.

Some disadvantages of reset control and specifically CR structure remain unsolved, one of them being the robustness to measurement noise [7]. The measurement noise present in the reset line, i.e., the signal whose zero-crossings determine the reset instants, can create unwanted excessive reset instants, which leads to performance deterioration. The lead filter used before the reset element in CR amplifies the high-frequency spectrum in the reset signal and worsens the problem [8]. Moreover, it has been shown that the steady-state performance of a CgLp-PID controlled system is deteriorated by quantization [9].

Frequency filters such as Low-Pass Filters (LPF) have been suggested as a noise filter for reset control by using them on the reset line [7, 8]. Although the high frequency noise is successfully reduced, the describing function (DF) gain and phase of the system are negatively influenced. Time regularization of the reset condition can also be used to reduce the effect of noise on the measurement signal [9]. However, it was shown that the sinusoidal tracking was only improved for a certain frequency band, which led the research towards observers as they may have less influence on the DF and are not

restricted in frequency domain [10].

Disturbance and state observers have been widely used in industry to filter noisy measurements and improve system performance [11, 12, 13]. State observers have been used in combination with reset control to estimate hidden states [14]. In addition, they can also be used to filter measurement noise. Since high tech industry requires high bandwidth frequencies for their motion stages, filters that depend upon heavy, real-time calculations are not applicable. The static Kalman filter is a less complicated filter that does not require real time parameter evaluations, so it remains as a possible solution for high tech systems.

This paper proposes a new control loop architecture that includes a separate feedback line for the calculation of the reset condition. A static Kalman filter is used on this separate feedback line to filter out the measurement noise. The aim is to improve the robustness of reset control elements to measurement noise and to reduce excessive resets. An analysis on the transient and steady-state performance of the control loop are done in simulations and experiments.

The remainder of this paper is structured as follows. In section 2 the preliminaries of reset control and the general observers are given. After this, the effect of measurement noise on reset control is shown in section 3. The proposed loop architecture and its stability conditions are presented in section 4 and an analysis on the closed-loop transient performance of the proposed architecture is done in section 5. The closed-loop steady-state performance is analyzed in section 6, and a practical example on a motion stage can be found in section 7. Finally, the conclusion of this paper is given in section 8.

2. Preliminaries

This section provides the preliminaries of the study.

2.1. Reset control

Reset control is a non-linear form of control that most commonly relies on a zero-crossing reset law. A general state space form is written down in (1) as a Single Input Single Output (SISO) system. It behaves as a linear system for non-zero input $e(t)$. When the input crosses zero, the state is 'reset' by means of the A_ρ matrix. Generally this matrix has a diagonal shape: $A_\rho = \text{diag}(\gamma_1, \gamma_2, ..., \gamma_n)$, with $\gamma_n \in [-1, 1]$. A reset time instance $t_k > 0$ is defined by $e(t_k) = 0$.

$$(R): \begin{cases} \dot{\mathbf{x}}_r(t) = A_r\mathbf{x}_r(t) + B_r e(t) & \text{if } e(t) \neq 0, \\ \mathbf{x}_r(t^+) = A_\rho \mathbf{x}_r(t) & \text{if } e(t) = 0, \\ u(t) = C_r\mathbf{x}_r(t) + D_r e(t). \end{cases} \tag{1}$$

The A_r, B_r, C_r, D_r matrices form the Base Linear System (BLS) of the reset control system.

2.2. Describing function

Non-linear systems cannot be cast into a linear frequency domain function, which causes design difficulties as an approximation has to be made. A quasi-linearization method, called the sinusoidal input Describing Function (DF) is used to approximate the behaviour of non-linear systems [15]. This allows industry to keep using loop-shaping method in frequency domain for the design of the non-linear controllers. However, the DF method only takes the first-order harmonic of the Fourier series into account and neglects higher-order harmonics. Approximation by only using the first-order can be significantly inaccurate [16, 17]. The Higher Order Sinusoidal Input Describing Function (HOSIDF) is used to calculate the higher-order harmonics of the output signal of non-linear controllers. The HOSIDF method for reset elements defined by (1) was introduced by [18, 19] as:

$$H_n(\omega) = \begin{cases} C_r(j\omega I - A_r)^{-1}(I + j\Theta(\omega))B_r + D_r, & n = 1 \\ C_r(j\omega I - A_r)^{-1} j\Theta(\omega) B_r, & \text{odd } n > 2 \\ 0, & \text{even } n \geq 2 \end{cases} \tag{2}$$

with,

$$\begin{aligned} \Theta(\omega) &= \frac{-2\omega^2}{\pi}\Delta(\omega)(\Gamma(\omega) - \Lambda^{-1}(\omega)) \\ \Lambda(\omega) &= \omega^2 I + A_r^2 \\ \Delta(\omega) &= I + e^{\frac{\pi}{\omega}A_r} \\ \Delta_r(\omega) &= I + A_\rho e^{\frac{\pi}{\omega}A_r} \\ \Gamma(\omega) &= \Delta_r^{-1}(\omega) A_\rho \Delta(\omega)\Lambda^{-1}(\omega). \end{aligned} \tag{3}$$

Where $H_n(\omega)$ is the n^{th} harmonic describing function.

2.3. Reset elements

Varying forms of reset elements can be described by the SISO system in (1). Reset control is originating from the resetting Clegg Integrator (CI) that was presented in [20]. The main advantage of adding the reset action is the increase in phase from $-90°$ to $-38°$, with

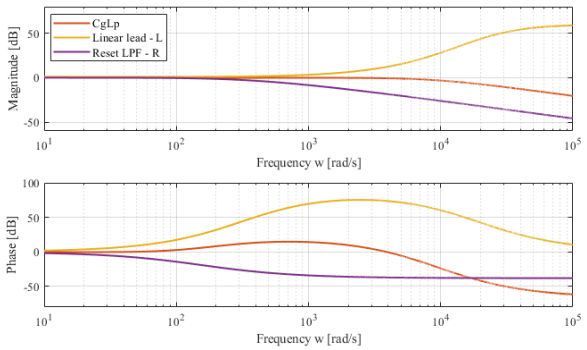

Figure 1: Broadband phase lead achieved with CgLp using FORE in range [$\omega_r = 172, \omega_f = 9420$] with $\gamma = 0$, and $\omega_{r\alpha} = 0.93\omega_r$

almost no increase in gain. This property is mainly used to increase the phase margin of a system. Later, the Clegg integrator was combined with linear elements to form a PI+CI structure, which uses a CI and a PI in parallel where the ratio between the two can be tuned [21]. The First-Order Reset Element (FORE) was introduced in [22] and additionally the Second-Order Reset Element (SORE) was first presented in [3]. These elements behave like a first- and second-order LPF, respectively, and provide the same phase advantage as the Clegg integrator in a range of frequencies.

In [5] the FORE and SORE were combined with a linear (tamed) lead filter to form the CgLp structure. It achieves a broadband phase lead while keeping the gain constant, which is visualized by the bode plot in Fig. 1. The CgLp element has a constant gain in the frequency range 100 − 3000 rad/s, while a phase lead of 15° is created. This would not be possible for linear control, as this behaviour does not adhere to Bode's gain-phase relationship. The general reset structure in (1) can be used to make a FORE based CgLp if the matrices are chosen as in (4).

$$\begin{aligned} A_r &= \begin{bmatrix} -\omega_{r\alpha} & 0 \\ \omega_f & \omega_f \end{bmatrix}, B_r = \begin{bmatrix} \omega_{r\alpha} \\ 0 \end{bmatrix}, \\ C_r &= \begin{bmatrix} \frac{\omega_f}{\omega_r} & (1 - \frac{\omega_f}{\omega_r}) \end{bmatrix}, D_r = [0], A_\rho = \begin{bmatrix} \gamma & 0 \\ 0 & 1 \end{bmatrix} \end{aligned} \tag{4}$$

Where $\omega_{r\alpha}$ is pole of the lag element, ω_r and ω_f are the zero and pole of the tamed lead element respectively. The CgLp element is used to partly replace the D action of the PID controller. For example, in [6] it is shown that the D action of the PID controller should be minimal to ensure stability of the BLS, and that the major phase lead should be provided by the CgLp element to ensure the best performance.

The previously mentioned reset elements all have

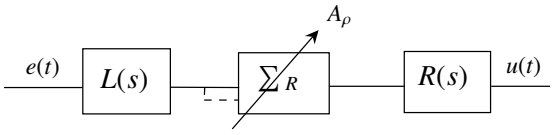

Figure 2: Block scheme of the CR structure [7].

a discontinuous output signal which creates practical problems when inputted to an actuator. Therefore, a different control architecture for reset elements was introduced to create a continuous output signal [7]. Furthermore, the architecture significantly improves the transient response in terms of overshoot and settling time.

The CR structure consists of a lead filter, reset element, and a lag filter in series as shown by Fig. 2. The lead and lag filters are defined by (5).

$$L(s) = \frac{s/\omega_l + 1}{s/\omega_h + 1}, \quad R(s) = \frac{1}{s/\omega_l + 1} \tag{5}$$

If ω_h is chosen to be relatively large enough with respect to the bandwidth frequency, the CR lead and lag filters cancel each other and almost do not influence the DF of the controller. With the same assumption, one can approximate the reset law by

$$e_r(t) = \dot{e}(t)/\omega_l + e(t) = 0. \tag{6}$$

It has been shown that the magnitude of higher-order harmonics is reduced by putting a reset element inside the CR structure. As a result, the first-order DF will be a better approximation of the actual controller and the result of the loop-shaping procedure is closer to ideal [7].

2.4. Observer theory

State estimators were introduced as a method to reconstruct hidden states of a process [23, 24, 25]. A state space system is used to estimate the process states and can also be used to filter out noise. Note the difference between the Luenberger observer and a static Kalman filter, since both state estimators use the exact same architecture and only the correction gain vector is calculated differently. A brief explanation which introduces the mathematics of a general observer in continuous time is given below.

Plant process. Assume that the plant process, which is required to be estimated, can be modeled as the state space system below.

$$\begin{aligned} \dot{x}_p &= A_p x_p + B_p u \\ y_p &= C_p x_p + D_p u \end{aligned} \tag{7}$$

Estimation. An estimation of the plant state is made by the observer using the plant model. The estimation is defined in (8).

$$\dot{\hat{x}} = A_L\hat{x} + B_L u + w_L \tag{8}$$

where $\hat{x}$ is the estimation of the true plant state x_p, and w_L is the process noise with $p(w_L) \sim N(0, Q)$, which is assumed to be normally distributed. Note that the actual plant process can differ from the model in the observer. In other words, the state space matrices $\{A_L, B_L, C_L, D_L\}$ are not necessarily equal to $\{A_p, B_p, C_p, D_p\}$.

Sensing. A sensor measurement z can be modelled as:

$$z = C_p x_p + D_p u + v_p. \tag{9}$$

where v_p is the measurement noise, which is assumed to be normally distributed: $p(v_p) \sim N(0, R)$.

Correction. Using the above, a correction on the state estimation is done based on the observer gain L multiplied by the estimation error

$$\dot{\hat{x}} = A_L\hat{x} + B_L u + L(z - \hat{y}). \tag{10}$$

And the observer output is calculated as in (11).

$$\hat{y} = C_L\hat{x} + D_L u \tag{11}$$

In order to improve, rather than degrade the performance when adding an observer to the control loop, close attention should be given to calculation of the observer gain vector. There is a known trade-off, higher observer gain results in faster convergence to real plant states and also means more influence of the measurement noise on the observed states. The problem of choosing L can be cast into a pole placement problem of the observer state transition matrix $(A_L - LC_L)$. If the set (A, C) is observable, there exists a vector L that can map the eigenvalues of the transition matrix everywhere in the complex plain. For stability reasons, these eigenvalues should be in the left half plain and shouldn't coincide with the eigenvalues of matrix A_L. The calculation of the observer gain can also be cast into a linear-quadratic regulator (LQR) problem that can be solved to obtain the optimal vector. This LQR problem comes down to solving a Riccati equation. The continuous time Riccati function for this observer gain is formulated as (12).

$$A_L^T P + PA_L - PC_L^T R^{-1} C_L P + Q = 0 \tag{12}$$

If (12) is solved for P, the optimal observer gain vector can be calculated by using $L = PC_L R^{-1}$. When measurement and process noise are assumed to be Gaussian distributed, the observer is also known as the static Kalman filter. If the covariance terms Q and R are time-variant and the gain is calculated real time, the observer is also known as the general Kalman filter.

The calculation of the observer gain from (12) is used in this paper to tune the observer, since it is also the optimal gain vector if model uncertainties do exist. Moreover, the knowledge about the model uncertainties be incorporated in the Q term of (12).

2.5. Pseudo-Sensitivity

For linear systems without feedback filters, the sensitivity is defined by (13).

$$S = \frac{1}{1 + C(s)P(s)} \tag{13}$$

However, this does not hold for non-linear controllers and a new definition is needed. In [19], the pseudo-sensitivity is defined as below.

$$|S_\infty(j\omega)| = \frac{\max\limits_{t>t_{ss}} |e(t)|}{|r(t)|} \tag{14}$$

where $r(t)$ and $e(t)$ are the reference and error, respectively. And t_{ss} is the first reset instant after steady-state.

3. Effect of noise on reset control

Performance degradation due to measurement noise has been reported for various control loops. For linear control, it mostly degrades the steady-state positioning and tracking since the accuracy is only limited by the noise level, i.e., the accuracy cannot be increased beyond the signal to noise ratio (SNR). For reset control, the zero-crossing detection is affected by the noise as well, which introduces extra degradation of the performance. Quantization is a specific form of measurement noise that is inherently connected to digital sensors. Given the quantization step size Δ, an error band is created on the reset condition of 0 to Δ. This can create faulty resets as the quantized measurement can be zero while the actual position is not zero [26].

Consider second-order plant to be controlled by a CR-CgLp-PID controller with 40° phase margin at a bandwidth frequency of 150 Hz. Let the plant be described by (15), which is the mass-spring-damper system that was fitted for a precision motion stage.

$$P(s) = \frac{8769}{s^2 + 43.99s + 7737} \tag{15}$$

When a linear increasing reference is chosen, limit cycles can be seen in the response when measurements

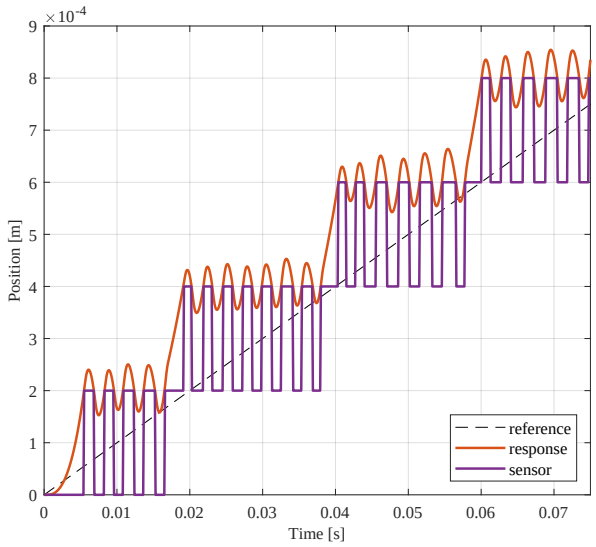

Figure 3: Limit cycles in the response, induced by the magnitude discretization of the sensor, $\Delta = 0.2$mm

are quantized. Fig. 3 also shows that for this non-linear controller, the magnitude of the limit cycles are not decaying.

When the measurement noise is considered to be additive and white, similar results are seen as the reset instances t_k are altered. Moreover, the noise not only creates different but also extra, excessive zero-crossings in the measurement signal. A sinusoidal error signal $e(t) = A\sin(\omega t)$ has two zero-crossings per period at $t_k = \frac{\pi k}{\omega}$, $k = [1, 2, 3, ...]$. One readily concludes that more zero-crossings per period are found in the same signal with additive white noise $e(t) = A\sin(\omega t) + d(t)$, with $d(t)$ $N(0, R)$. Furthermore, excessive resets especially occur when the original signal is small relative to the noise variance and the original reset instants are not necessarily zero-crossings anymore. Fig. 4 shows the excessive resets for CR-CgLp-PID and CgLp-PID controllers when a reference of 10 Hz is given. For the control loops without noise, periodic resets are seen. For the loops with noise, the reset condition is triggered excessively. The difference between the CR-CgLp-PID and CgLp-PID can also be observed. The extra lead filter in the CR structure is amplifying high frequencies, causing even more resets than the CgLp-PID controller.

An illustration of the effects of those excessive resets on the tracking performance is given in the pseudo-sensitivity plot in Fig. 5, in which a mass-spring-damper plant is controlled by a PID, a CgLp-PID, and a CR-CgLp-PID controller. All three controllers were tuned to have the same phase margin of 40° at bandwidth frequency of 150 Hz. Additive white noise with $P_n = 2e^{-12}$ W and a reference amplitude of $A_{ref} = 300$ μm are used. Fig. 5 shows that the response of the linear controller converges to the SNR of -46.5 dB for low frequencies. Note that the non-linear controllers have an even higher minimum at low frequencies and therefore their performance is degraded more than that of linear controller.

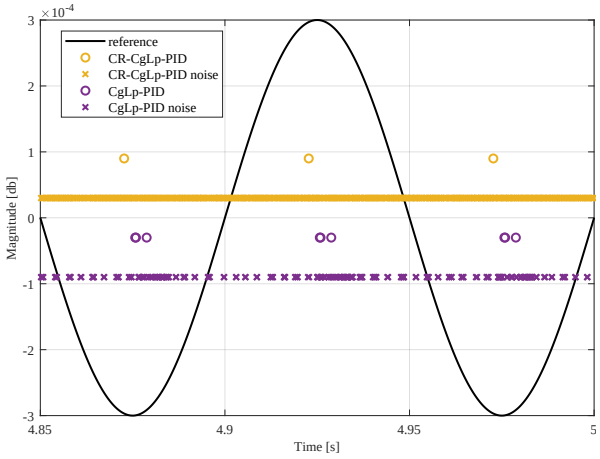

Figure 4: Reset instances of two controllers with and without white noise, $P_n = 2e^{-12}$ W, $f_{ref} = 10$ Hz

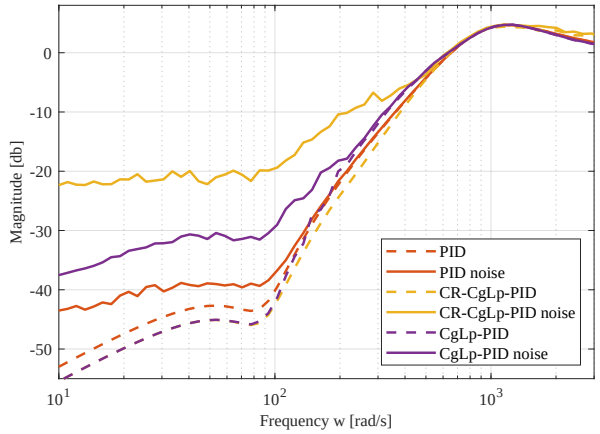

Figure 5: Pseudo-sensitivity of linear and non-linear controllers with and without white noise, $P_n = 2e^{-12}$ W, $A_{ref} = 300$ μm

A similar conclusion is drawn when the transient performance is analyzed. Fig. 6 shows the step response for the same control loops with and without the white noise. The step response of the PID controller is not affected by the noise, whereas both reset controllers perform worse when fed with noisy measurements. The CR-CgLp-PID controller shows a large overshoot which

decays very slow, making the controller unsuitable for practical implementations.

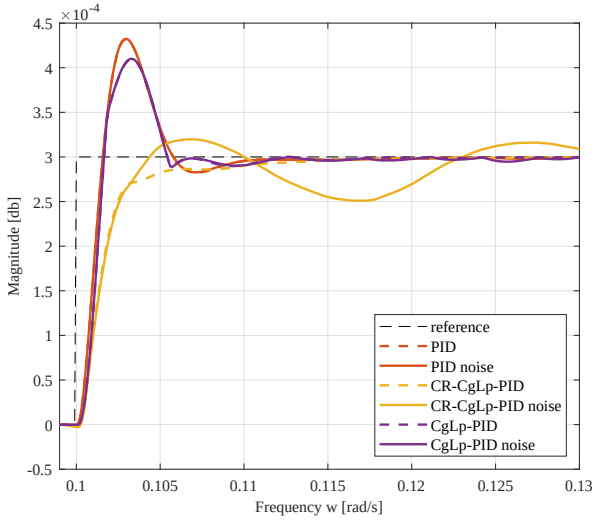

Figure 6: Step response of linear and non-linear controllers with and without white noise, $P_n = 2e^{-12}$ W

A couple of mitigations for these problems were proposed in literature. For quantization noise specifically, a time regularization has been proposed to cap the amount of reset instances per time period [9]. By using a LPF to filter e_r, general high frequency noise can be removed [7, 8]. These mitigations were able to reduce the amount of excessive resets, but their main disadvantage is the phase increase in the DF of the Open Loop (OL). This conflicts with the main purpose of adding phase margin that the reset controllers were introduced for.

4. Proposed control loop architecture

The new control loop architecture that this paper proposes, consists of a separated feedback line to the reset line of the CR-CgLp-PID controller. This separate reset feedback line is filtered by an observer to reduce the amount of excessive resets by filtering the noise out of the measurement signal. A schematic overview of the proposed architecture can be seen in Fig. 7. The open loop is not changed with respect to the architecture in [7]. A lead and lag element, i.e., $L(s)$ and $R(s)$, are placed in front and after the FORE-CgLp reset element respectively to form a CR structure. The HOSIDF of the CR-CgLp-PID controller is shown in Fig. 8. It can be seen that the higher-order harmonics are relatively low with respect to the first harmonic and that the controller provides 40° phase at $\omega_{BW} = \omega_c = 150$ Hz. In this new

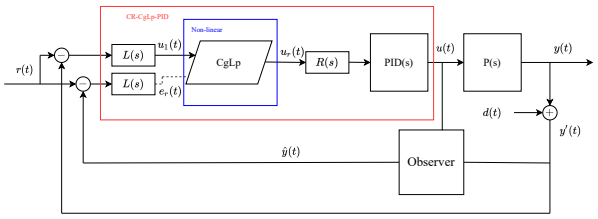

Figure 7: The proposed control loop with the observer on the reset line

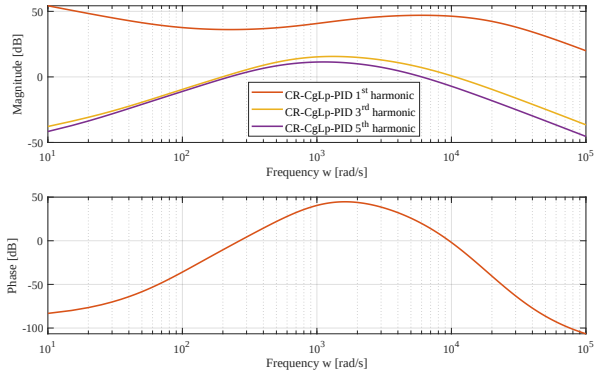

Figure 8: HOSIDF of the CR-CgLp-PID controller, $\omega_r = \omega_{r\alpha} = \omega_c = 942$ rad/s, $\omega_f = \omega_h = 20\omega_c$, $\omega_l = \omega_c/3$, $\gamma = 0$.

loop architecture, the reset condition has changed from (6) to (16).

$$e_r(t) = \dot{\hat{e}}(t)/\omega_l + \hat{e}(t) = 0 \tag{16}$$

where $\hat{e}(t) = r(t) - \hat{y}(t)$. The main motivation for this change is that the observer output $\hat{y}(t)$ is less deteriorated by the measurement noise than the plant output $y(t)$.

While the reset feedback line is filtered by the observer, the general feedback line is kept intact. Noise is therefore still influencing the error that is fed to the controller. If the observer is also placed on the general feedback line, noise could be completely filtered out in theory. However, the dependence of the observer on the correctness of the state space matrices is critical. Wrong estimation of the parameters causes performance issues in that configuration. On the reset feedback line, only the zero-crossings are used to calculate the control output. It will be shown later that the proposed configuration is more robust to model inaccuracies.

4.1. Stability of the proposed control loop

In this section stability conditions are given for the proposed control loop. The stability of reset control systems has been investigated thoroughly in literature

[6, 19, 27, 28, 29]. Previous work is exploited to prove the stability for the proposed system. Consider the proposed architecture from Fig. 7 and let it be separated in a linear and a non-linear part. The non-linear part can be described by (17), with inputs $u_1(t), e_r(t)$ and output $u_r(t)$.

$$(R): \begin{cases} \dot{\mathbf{x}}_r(t) = A_r\mathbf{x}_r(t) + B_r u_1(t) & \text{if } e_r(t) \neq 0, \\ \mathbf{x}_r(t^+) = A_\rho \mathbf{x}_r(t) & \text{if } e_r(t) = 0, \\ u_r(t) = C_r\mathbf{x}_r(t) + D_r u_1(t). \end{cases} \quad (17)$$

The linear system is described by (18) with input u_r, disturbance $w(t) = \begin{bmatrix} r(t) & d(t) \end{bmatrix}$, and output y, e_r, u_1 [19].

$$(\mathcal{L}): \begin{cases} \dot{\zeta}(t) = A\zeta(t) + B_u u_r(t) + Bw(t) \\ y(t) = C\zeta(t) \\ e_r(t) = C_e\zeta + D_{ue}u_r(t) + D_e w(t) \\ u_1(t) = C_1\zeta + D_{u1}u_r(t) + D_1 w(t) \end{cases} \quad (18)$$

In which ζ is containing the controller, plant, and observer states. Both systems can be combined to retrieve the closed-loop state space representation of the overall system that can be written as (19).

$$\begin{cases} \dot{\mathbf{x}}(t) = \bar{A}\mathbf{x}(t) + \bar{B}w(t) & \text{if } e_r(t) \neq 0, \\ \mathbf{x}(t^+) = \bar{A}_\rho \mathbf{x}(t) & \text{if } e_r(t) = 0, \\ y(t) = \bar{C}\mathbf{x}(t) \\ e_r(t) = \bar{C}_e\mathbf{x}(t) + \bar{D}_e w(t) \end{cases} \quad (19)$$

Where $x(t) = \begin{bmatrix} \mathbf{x}_r(t)^T & \zeta(t)^T \end{bmatrix}^T$, $\bar{A} = \begin{bmatrix} A_r + B_r D_{u1} C_r & B_r C_1 \\ B_u C_r & A \end{bmatrix}$, $\bar{B} = \begin{bmatrix} B_r D_1 \\ B_u D_1 \end{bmatrix}$, $\bar{C} = \begin{bmatrix} 0 & C \end{bmatrix}$, $\bar{C}_e = \begin{bmatrix} 0_{1\times n_r} & C_e \end{bmatrix}$, $\bar{D}_e = D_e$, $\bar{A}_\rho = \begin{bmatrix} A_\rho & 0 \\ 0 & I \end{bmatrix}$, and including that $D_p = D_r = D_{ue} = \mathbf{0}$.
When studying the stability of the unforced system by assuming $w(t) = 0$, it is concluded that $\hat{y} = y' = y$ if the observer matrices are matching the plant. If they differ from the actual plant state-space matrices, the well-posedness property of the reset instances are preserved if the observer is stable, implicating that all eigenvalues of the state transition matrix of the observer $(A_L - LC_L)$ are located in the left half plane.

Hence, the quadratic stability can be guaranteed if the H_β condition is satisfied for the system without observer [19]. The H_β-condition can be used to prove that the zero equilibrium of the reset control system with $r(t) = w(t) = 0$ is quadratically stable [19, 28, 30]. The H_β-condition is briefly recalled in Theorem 1.

Theorem 1. *The unforced reset control system* (19) *is quadratically stable if and only if there exist* $\beta \in \mathbb{R}^{n_r\times 1}$ *and* $\rho = \rho^T > 0$, $\rho \in \mathbb{R}^{n_r\times n_r}$, *such that*

$$H_\beta(s) = C_0(sI - \bar{A})^{-1}B_0 \quad (20)$$

is strictly positive real (SPR), the set $(\bar{A}, B_0)$ *and* $\bar{A}, C_0$ *are controllable and observable respectively, with*

$$C_0 = \begin{bmatrix} \rho & \beta C \end{bmatrix}, \quad B_0 = \begin{bmatrix} I_{n_r\times n_r} \\ 0_{n_p\times n_r} \end{bmatrix}, \quad (21)$$

and

$$A_\rho^T \rho A_\rho - \rho < 0. \quad (22)$$

Definition 1. *The reset control system* (19) *is uniformly bounded-input bounded-state (UBIBS) stable if for each* $\eta > 0$, *there exists* $\mu > 0$ *such that for each initial condition* x_0 *and each bounded input* $w(t)$, *the solution* $x(t, x_0, w)$ *continues over* $\mathbb{R}^+$ *and*

$$\|x_0\| < \eta, \quad \|w\|_\infty < \eta \Rightarrow \|x(t, x_0, w)\| < \mu$$

for all $t \geq 0$.

For the system (19), when $w(t) \neq 0$, a similar approach as the proof of Theorem 13 in [28] is given to proof UBIBS stability of (19) on the condition that the unforced system is quadratically stable.

Proof. A new system is defined as:

$$z(t) = x(t) - x_l(t), \quad (23)$$

in which $x_l(t)$ denotes the base linear system. The dynamics of $z(t)$ satisfy:

$$\begin{cases} \dot{z}(t) = \bar{A}z(t), & e_r \neq 0 \\ z(t^+) = \bar{A}_\rho x(t) - x_l(t) & e_r = 0 \\ e_r(t) = \bar{C}_e x(t) + \bar{D}_e w(t). \end{cases} \quad (24)$$

Where $z(t) = \begin{bmatrix} z'_{\bar{\rho}}(t) & z'_\rho(t) \end{bmatrix}'$. Here $z_{\bar{\rho}}(t)$ and $z_\rho(t)$ denote the states that are not reset and the states that are reset, respectively. Similar to [28], for UBIBS stability it is sufficient to show that $\left\|z_{\bar{\rho}}(t)\right\| + \left\|z_\rho(t)\right\|$ is bounded.

Now the quadratic Lyapunov function $V(t) = z'(t)Pz(t)$ can be considered and used to conclude that $\left\|z_{\bar{\rho}}(t)\right\| + \left\|z_\rho(t)\right\|$ is bounded. We can partition [19]

$$P = \begin{bmatrix} P_1 & (\beta C_e)^T \\ \beta C_e & \rho \end{bmatrix} \quad (25)$$

with $P_1 > 0$. By using the KYP Lemma and for $t \in (t_i, t_{i+1}]$, we compute (26) [28].

$$\dot{V}(t) = z'(t)(-qq' - \epsilon P)z(t) \leq -\epsilon V(t) \quad (26)$$

Thus,

$$V(t) \leq e^{\epsilon(t-t_i)} V(t_i^+), \quad t \in (t_i, t_{i+1}] \tag{27}$$

Therefore we consider the Lyapunov function at reset instance and we can then write

$$V(t) = z'_{\bar{\rho}}(t) P_1 z_{\bar{\rho}}(t) + 2 z'_{\rho}(t) \beta C_e z_{\bar{\rho}}(t) + z'_{\rho}(t) z_{\rho}(t) \tag{28}$$

Evaluating at $t = t_i^+$ we derive

$$V(t_i^+) \leq V(t_i) + 2 \left\| x_{\rho}(t_i) \right\| \left(\left\| \beta C_e z_{\bar{\rho}}(t_i) \right\| + \left\| x_{\rho l}(t_i) \right\| \right). \tag{29}$$

Since the BLS is stable, we conclude that $\left\| x_{\rho l}(t_i) \right\|$ is bounded. Next it is shown that the term $\left\| \beta C_e z_{\bar{\rho}}(t_i) \right\|$ is bounded by recalling the reset condition at reset instance $e_r(t_i^+) = \bar{C}_e x(t_i^+) + \bar{D}_e w(t_i^+) = 0$. Since the reset condition is not a function of the resetting states

$$-D_e w(t_i^+) = C_e x_{\bar{\rho}}(t_i^+) = C_e z_{\bar{\rho}}(t_i^+) + C_e x_{\bar{\rho} l}(t_i^+). \tag{30}$$

Thus,

$$\left\| C_e z_{\bar{\rho}}(t_i^+) \right\| \leq \left\| D_e w(t)_i^+ \right\| + \left\| C_e x_{\bar{\rho} l}(t_i^+) \right\|. \tag{31}$$

Since the input $w(t)$ is bounded by definition, and again $\left\| x_{\bar{\rho} l}(t) \right\|$ is bounded because the BLS is stable, we conclude that $\left\| C_e z_{\bar{\rho}}(t) \right\|$ is bounded as well. The rest of the proof including the boundedness of $\left\| x_{\rho}(t) \right\|$ is already done in [28]. □

From the stability analysis above, it can be concluded that a shaping filter $C_s(s)$ on the reset line would not endanger the stability of the overall system. This was briefly mentioned in [28] as the independence of the method on the reset instances, but refuted by [19]. However, only the reset condition $e_r(t)$ is depending on the shaping filter, and it will not make (26) unbounded. Since the stability conditions are derived, the rest of the paper focuses on the performance of the proposed control loop.

4.2. Control output

In order to illustrate that the continuous output of the CR-structure is maintained in the proposed control loop and that it still has a feasible output, it is compared with conventional architectures. Fig. 9 shows the control output $u(t)$ for a sinusoidal reference at low frequency: $r(t) = 3e^{-4} \sin 63t$. White noise with $P_n = 2e^{-12}$ W is added to the measurement: $y' = y + d(t)$. It can clearly be seen that the power output of the CR-based structures is much less than the CgLp only. Furthermore, the proposed architecture also improves upon the conventional CR-CgLp-PID and PID loops. The new architecture with observer has a RMS value of $2.3e^{-4}$ whereas the

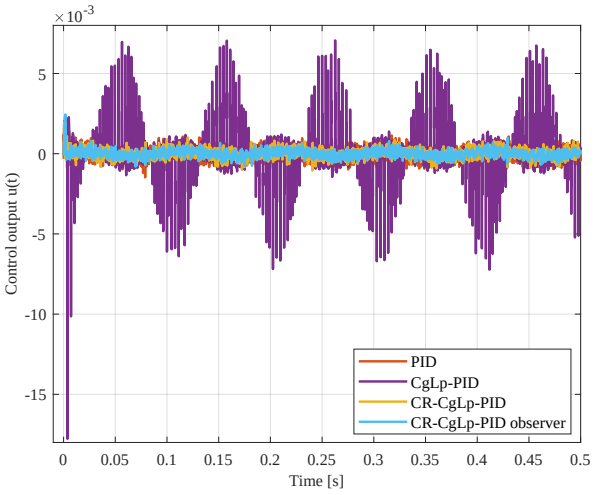

Figure 9: Control output of PID, CgLp-PID, CR-CgLp-PID, and the proposed control loop to a sinusoidal reference, with $r(t) = 3e^{-4} \sin 63t$

CR-CgLp-PID and PID controllers output a signal with RMS $2.8e^{-4}$ and $3.6e^{-4}$, respectively. Fig. 10 shows the control signal when a reference of $r(t) = 3e^{-4} \sin 942t$ is given to the system. At this bandwidth frequency, it is seen that the sharp peaks in the control output are removed when using a CR structure. The output of the CR structure is much smoother than the CgLp controller. The proposed control loop therefore has lower higher-order harmonics than the CgLp-PID controlled loop. In addition, the proposed control loop shows the same response as the other CR controlled loops.

5. Closed-loop transient performance

The closed-loop transient performance is analyzed by numerical simulations. The details of the simulation parameters can be found in Appendix A.

5.1. Noise case

Consider the closed-loop system as shown in Fig. 7, including white additive sensor noise $d(t)$ with noise power $P_n = 2e^{-12}$ W. The plant is modelled as the second-order mass-spring-damper system (15). The proposed control loop is compared with a standard PID controller and a CgLp-PID controller which are tuned for the same bandwidth frequency of 150 Hz and phase margin of 40°. The observer is modelled as in (10). The step response of the control loops can be seen in Fig. 11. For comparison, an ideal case is added in which no noise is added to the reset feedback line. The proposed control loop removes the large overshoot and oscillations that were caused by the measurement noise.

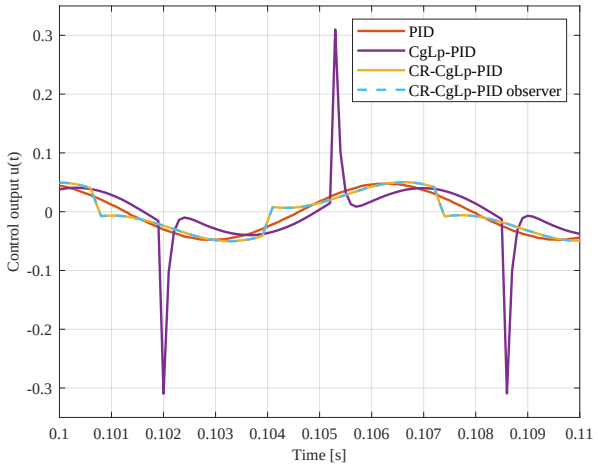

Figure 10: Control output of PID, CgLp-PID, CR-CgLp-PID, and the proposed control loop to a sinusoidal reference, with $r(t) = 3e^{-4} \sin 942t$

Besides this, the settling time is decreased drastically with respect to the other controllers. There is almost no difference between the ideal case and the proposed control loop, which implicates that the observer is correctly filtering the measurement signal.

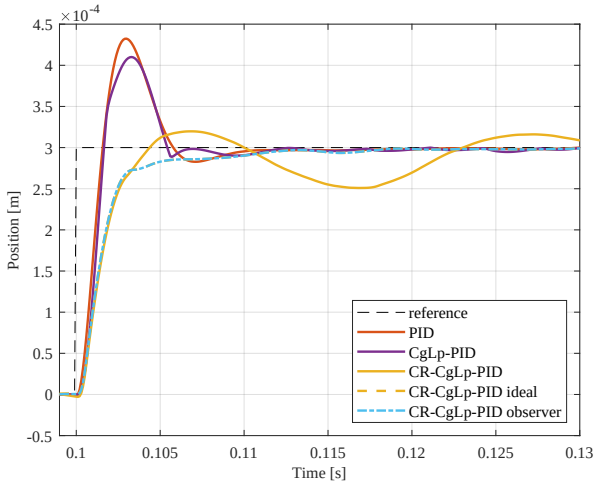

Figure 11: Step response of the proposed control loop with and without using an observer, white additive measurement noise with $P_n = 2e^{-12}$ W

5.2. *Model inaccuracy case*

The previous simulation case proves the theoretically possible improvements of the transient performance, but it remains an ideal case since the state space matrices of the observer are exactly matching the plant process. Therefore, a non-ideal case is considered in which the state space matrices of the observer and the actual plant process are intentionally mismatched. The location of the resonance peak of the mass-spring-damper system ω_n is increased by 5%. No noise is added to the measurements to clearly isolate the effects of the model mismatch. It can be seen in Fig. 12 that the step response of the proposed system shows a little overshoot due to the model mismatch, but the performance remains very similar with respect to the CR-CgLp-PID controller without observer. It can be concluded that the observer with a model mismatch does not degrade the transient performance with respect to the conventional CR-CgLp-PID controller.

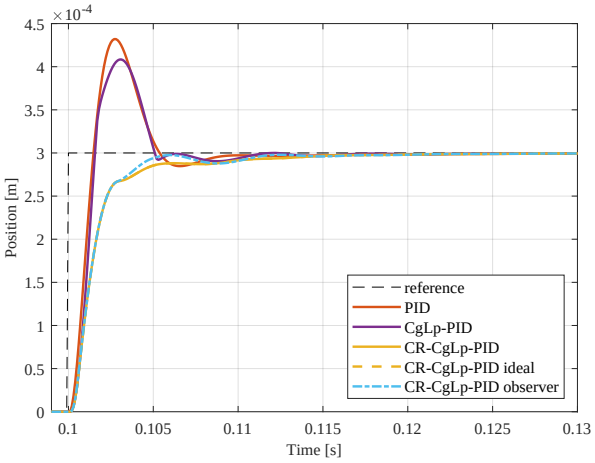

Figure 12: Step response of the proposed control loop with and without using an observer, in which $\omega_n = 1.05\omega_n$

6. Closed-loop steady-state performance

The closed-loop steady-state performance is analyzed by numerical simulations. The details of the simulation parameters can be found in Appendix A.

6.1. *Noise case*

Again consider the same control loops and the same additive white noise. A sinusoidal reference with amplitude $A_{ref} = 300$ μm, was used to generate the pseudo-sensitivity plot in Fig. 13. The minimum that was also observed in Fig. 5 is reduced when using the proposed control loop. Without the observer, a minimum in pseudo-sensitivity occurs at -23 dB. When the correct model of the plant is given to the observer, sinusoidal tracking can be improved to -36 dB. Again the proposed control loop is also compared to a control loop in which the reset feedback line is not deteriorated by

noise. It can be seen that by using the observer a similar performance can be obtained as the ideal case.

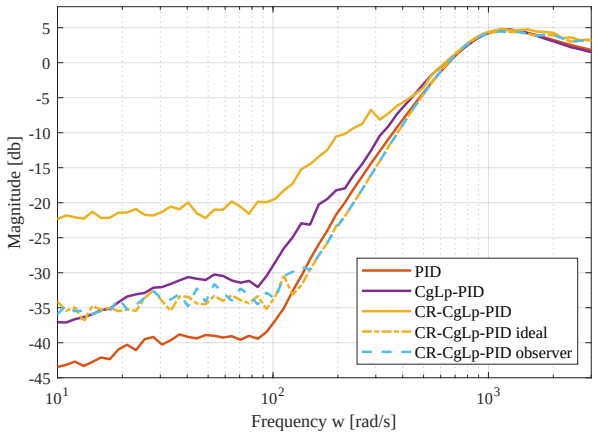

Figure 13: Pseudo-sensitivity of the proposed control loop with and without using an observer, white additive noise with $SNR = 46.5$ dB

6.2. *Model inaccuracy case*

The steady-state performance improvement of the proposed control loop is again theoretically shown in the previous section. This section considers a situation in which the model of the observer is inaccurate and steady-state performance is analyzed. When the sensitivity of the control loop is calculated by means of the closed loop state space equations in (19), the reset line and therefore the observer inaccuracy are not incorporated. In order to integrate the observer inaccuracies in the sensitivity analytically, a new OL is calculated using a shaping filter that approximates the phase shift caused by the separated reset feedback line with the observer. With this method, the DF of the OL can be calculated using the conventional HOSIDF methods and used to calculate the sensitivity.

Again the resonance frequency of (15) is increased by 5% in the simulation. The phase of this shaping filter is approximated by the phase difference of the error and the reset error line in the proposed control loop as described by (32).

$$\Delta\phi = \phi_{e_r} - \phi_e \tag{32}$$

Both phases can be calculated with respect to the input $r(t)$ by means of the transfer functions (33) and (34). In these transfer functions, the reset system (17) is approximated by its BLS and the noise is assumed to be zero.

$$e(t) = r(t) - y(t) = \left(1 - \frac{Y(s)}{R(s)}\right) r(t) \tag{33}$$

$$e_r(t) = r(t) - \hat{y}(t) = \left(1 - \frac{\hat{Y}(s)}{U(s)} P(s)^{-1} \frac{Y(s)}{R(s)}\right) r(t) \tag{34}$$

Fig. 14 shows the phases of the two error signals and

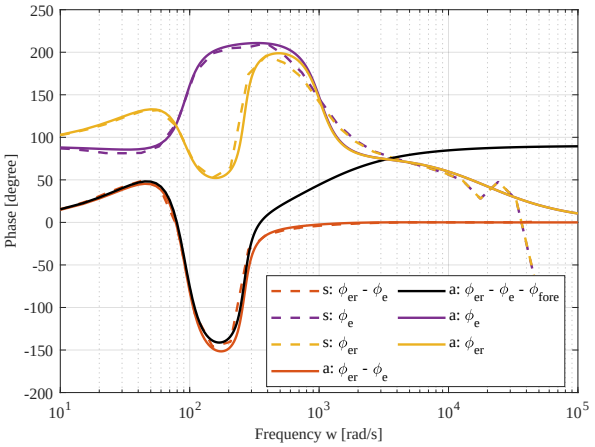

Figure 14: Phase shift in the error signals of the proposed control loop with model inaccuracy of $\omega_n = 1.05\omega_n$. Simulation results are denoted by s, analytical results denoted by a

their difference. Simulation results and analytical calculated lines are included and denoted with s and a respectively and show that a significant phase shift is created by the observer. Using this phase shift, a OL bode plot is calculated for the model inaccuracy case by implementing this phase shift as a shaping filter.

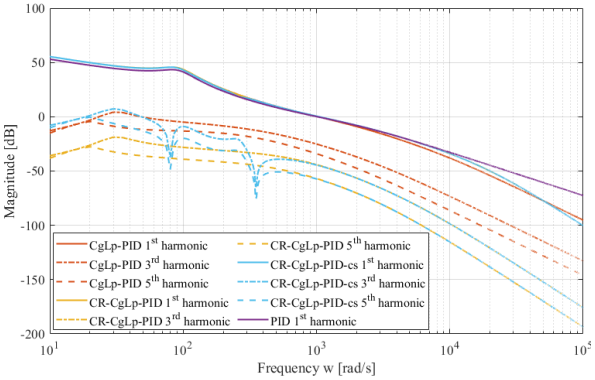

Figure 15: Open-loop bode plot of the proposed control loop with higher-order harmonics, and with approximated shaping filter

An increase in higher-order harmonics is caused by the observer with model inaccuracy, as can be seen in Fig. 15. The notches in the higher-order harmonics can be explained by analyzing the difference between $\Delta\phi$ and the phase of the reset element. This is visualized by the black line in Fig. 14. The notches are created when the reset instances coincide with the zero-crossings of

the state, and as a result the state is reset from zero to zero. This happens if the phase difference between the FORE element and the shaping filter is equal to an integer multiple of pi. In those cases, the system behaves entirely linear as the resets do not affect the output and the higher-order harmonics are therefore zero.

The first-order OL magnitude is used to calculate a sensitivity that approximates the pseudo-sensitivity that is be retrieved by numerical simulations. A comparison between the two is made in Fig. 16. It is observed that the sensitivity remains similar to the original sensitivity. However, small increases can be seen at the locations where the higher-order harmonics are increased. At these locations, the first-order harmonic is also increasing the sensitivity slightly. Besides this, the pseudo-sensitivity remains very similar to the original case without observer. It is therefore concluded that the proposed control loop is robust to resonance frequency shifts up to at least 5%.

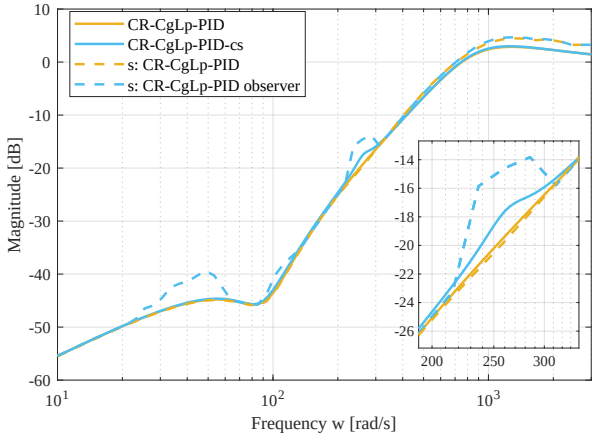

Figure 16: (Pseudo-)sensitivity of the proposed control loop with and without using an observer, in which $\omega_n = 1.05\omega_n$. Simulation results are denoted by s

7. Experimental setup

At the time of printing, the experiments were ongoing but not yet finished. Very early results seem to be backing the analytical and numerical work of this paper.

8. Conclusion

While the required accuracy demands in industry keep increasing, the linear PID controller performance is limited by the waterbed effect. Reset control can break this waterbed effect by using for example the CR-CgLp-PID controller architecture. Despite improvements, the CR based controller shows minimal robustness to noise. The high frequency content of noise present in the reset line causes unwanted excessive resets which degrade the overall performance of the reset controller.

This paper proposed an observer based solution that does not harm the phase of the DF, contrary to prior solutions that were suggested in literature. The presented solution consists of a separate feedback line for the reset condition that is filtered by an observer. Stability conditions based on the H_β-condition of derived in previous work was altered to apply to the new control loop architecture with the observer.

Transient and steady-state tracking were analysed in numerical simulations, in which the proposed control loop was compared with conventional linear and reset control. The proposed architecture showed a decrease in overshoot and lower settling time with respect to the conventional CR controller architecture when measurement noise was included. In addition, the pseudo-sensitivity was reduced by 13 dB at low frequencies without compromising the phase margin of the system. Analytical work and simulations showed normal robustness to parameter uncertainty in the observer. The RMS of the control output during low frequency tracking was decreased by 15% with respect to the conventional CR-structure.

By using an observer to filter out measurement noise on the reset feedback line, the transient and steady-state performance of CR-CgLp in sub-optimal environments was improved. Therefore this paper provides a solution that brings reset control closer to implementation in the high-tech industry.

Appendix A. Simulation parameters

Separated by each controller parameters, and the general parameters of the simulation.

Table A.1: Numerical simulation parameters CR-CgLp-PID

Parameter	Value	Unit
ω_{BW}	942	rad/s
ω_r	942	rad/s
$\omega_{r\alpha}$	942	rad/s
ω_f	18840	rad/s
γ	0	-
P	54.4919	-
ω_i	94.2	rad/s
ω_d	517.5824	rad/s
ω_t	1714.4	rad/s
ω_l	314	rad/s
ω_h	18840	rad/s

Table A.2: Numerical simulation parameters CgLp-PID

Parameter	Value	Unit
ω_{BW}	942	rad/s
ω_r	172	rad/s
$\omega_{r\alpha}$	170	rad/s
ω_f	9420	rad/s
γ	0.54	-
P	54.4919	-
ω_i	94.2	rad/s
ω_d	570.9091	rad/s
ω_t	1554.3	rad/s

Table A.3: Numerical simulation parameters PID

Parameter	Value	Unit
ω_{BW}	942	rad/s
P	41.0851	-
ω_i	94.2	rad/s
ω_d	387.3030	rad/s
ω_t	2291.1	rad/s

.

Table A.4: Numerical simulation parameters, simulation

Parameter	Value	Unit
f_s	10^4	Hz
Solver	ode1	-
A_{ref}	300	μm
P_n	$2e^{-12}$	W
n	100	-
f_{ref}	$1 - 10^4$	Hz

.

References

[1] R. Schmidt, G. Schitter, A. Rankers, J. van Eijk, The design of high performance mechatronics: high-tech functionality by multidisciplinary system integration, 2nd Edition, IOS Press, Netherlands, 2014. doi:10.3233/978-1-61499-368-1-i.

[2] O. Beker, C. Hollot, Y. Chait, Plant with integrator: an example of reset control overcoming limitations of linear feedback, IEEE Transactions on Automatic Control 46 (11) (2001) 1797–1799. doi:10.1109/9.964694.

[3] H. N. L.Hazeleger, M. Heertjes, Second-order reset elements for stage control design, Proceedings of the American Control Conference 2016-July (2016) 2643–2648. doi:10.1109/ACC.2016.7525315.

[4] Y. W. D. Wu, G. Guo, Reset integral-derivative control for hdd servo systems, IEEE Transactions on Control Systems Technology 15 (2007) 161–167. doi:10.1109/TCST.2006.883230.

[5] N. Saikumar, R. K. Sinha, S. H. HosseinNia, 'constant in gain lead in phase' element-application in precision motion control, IEEE/ASME Transactions on Mechatronics 24 (2019) 1176–1185. doi:10.1109/TMECH.2019.2909082.

[6] A. A. Dastjerdi, N. Saikumar, S. H. HosseinNia, Tuning of a class of reset elements using pseudo-sensitivities, in: European Control Conference (ECC), 2021, pp. 1187–1192. doi:10.23919/ECC54610.2021.9654942.

[7] N. Karbasizadeh, S. H. HosseinNia, Continuous reset element, arXiv preprint arXiv:2110.12801 (2021).

[8] C. Cai, A. A. Dastjerdi, N. Saikumar, S. HosseinNia, The optimal sequence for reset controllers, European Control Conference (ECC) (2020).

[9] B. Kieft, S. H. HosseinNia, N. Saikumar, Time regularization as a solution to mitigate quantization induced performance degradation, in: 2021 European Control Conference (ECC), 2021, pp. 2458–2464. doi:10.23919/ECC54610.2021.9655182.

[10] S. Shaik, J. Popat, T. K. Kumar, Kalman filter based phase delay reduction technique, 2016 International Conference on Recent Trends in Information Technology, ICRTIT (2016) 1–5doi:10.1109/ICRTIT.2016.7569549.

[11] R. Miklosovic, A. Radke, Z. Gao, Discrete implementation and generalization of the extended state observer, Proceedings of the American Control Conference 2006 (2006) 2209–2214. doi:10.1109/acc.2006.1656547.

[12] D. Yoo, S. S. Yau, Z. Gao, Optimal fast tracking observer bandwidth of the linear extended state observer, International Journal of Control 80 (2007) 102–111. doi:10.1080/00207170600936555.

[13] Y.-D. Yoon, E. Jung, A. Yoo, S.-K. Sul, Dual observers for the disturbance rejection of a motion control system, IEEE Industry Applications Annual Meeting (2007).

[14] H. Li, C. Du, Y. Wang, Optimal reset control for a dual-stage actuator system in hdds, IEEE/ASME Transactions on Mechatronics 16 (2011) 480–488. doi:10.1109/TMECH.2011.2123104.

[15] Y. Guo, W. Gui, C. Yang, L. Xie, Stability analysis and design of reset control systems with discrete-time triggering conditions, Automatica 48 (2012) 528–535. doi:10.1016/j.automatica.2011.12.001.
URL http://dx.doi.org/10.1016/j.automatica.2011.12.001

[16] E. Akyiiz, N. Saikumar, S. H. HosseinNia, Reset control for vibration disturbance rejection, IFAC-PapersOnLine 52 (2019) 525–530. doi:10.1016/j.ifacol.2019.11.729.

[17] N. Karbasizadeh, A. A. Dastjerdi, N. Saikumar, D. Valerio, S. H. HosseinNia, Benefiting from linear behaviour of a nonlinear reset-based element at certain frequencies, 2020 Australian and New Zealand Control Conference, ANZCC 2020 (2020) 226–231doi:10.1109/ANZCC50923.2020.9318363.

[18] N. Saikumar, K. Heinen, S. H. HosseinNia, Loop-shaping for reset control systems, Control Engineering Practice 111 (2021) 104808. doi:10.1016/j.conengprac.2021.104808.

[19] A. A. Dastjerdi, A. Astolfi, N. Saikumar, N. Karbasizadeh, D. Valerio, S. H. HosseinNia, Closed-loop frequency analysis of reset control systems, IEEE transactions on automatic control (in press).

[20] J. C. Clegg, A nonlinear integrator for servomechanisms, Transactions of the American Institute of Electrical Engineers, Part II: Applications and Industry 77 (1958) 41–42. doi:10.1109/tai.1958.6367399.

[21] A. Baños, A. Vidal, Design of reset control systems: The pi plus ci compensator, Journal of Dynamic Systems Measurement and Control 134 (2012) 051003/1–11. doi:10.1115/1.4004773.

[22] I. Horowitz, P. Rosenbaum, Non-linear design for cost of feedback reduction in systems with large parameter uncertainty, International Journal of Control 21 (1975) 977–1001. doi:10.1080/00207177508922051.

[23] R. E. Kalman, A new approach to linear filtering and prediction problems, ASME - Journal of Basic Engineering 82 (1960) 35–45.

[24] D. G. Luenberger, Observing the state of a linear system, IEEE Transactions on Military Electronics 8 (1964) 74–80. doi:10.1109/TME.1964.4323124.

[25] J. Farrell, 4 State Estimation, Academic press, 2005.

[26] B. Kieft, S. H. HosseinNia, N. Saikumar, Reset band for mitigation of quantization induced performance degradation, in: 2021 European Control Conference (ECC), 2021, pp. 2465–2472. doi:10.23919/ECC54610.2021.9654970.

[27] H. Hu, Y. Zheng, Y. Chait, C. Hollot, On the zero-input stability of control systems with clegg integrators, Proceedings of the 1997 American Control Conference (Cat. No.97CH36041) 1 (1997) 408–410 vol.1. doi:10.1109/ACC.1997.611829.

[28] O. Beker, C. V. Hollot, Y. Chait, H. Han, Fundamental properties of reset control systems, Automatica 40 (2004) 905–915. doi:10.1016/j.automatica.2004.01.004.

[29] A. Baños, J. Carrasco, A. Barreiro, Reset times-dependent stability of reset control systems, IEEE Transactions on Automatic Control 56 (2011) 217–223. doi:10.1109/TAC.2010.2088892.

[30] Y. Guo, L. Xie, Y. Wang, Analysis and Design of Reset Control Systems, Institution of Engineering and Technology, 2015. doi:10.1049/PBCE094E.

7

Conclusion

While the required accuracy demands in industry keep increasing, the linear PID controller performance is limited by the waterbed effect. Research is therefore done in utilizing non-linear control algorithms, such as reset elements. Since Bode's phase gain relationship does not apply to reset control, a phase lead band can be created while the gain is kept constant. The CgLp-PID and CR-CgLp-PID controllers have been shown to improve control performance in steady-state and transient performance upon linear elements. Despite their improvements with respect to linear control, both architectures have a lack of robustness to measurement noise. The noise present in the reset line creates excessive resets which degrade the transient and steady-state reset controller performance. Larger overshoot and an increase in tracking error are seen when the control system includes noise. As a result, the performance of the CgLp based controllers is far from ideal in experimental setups preventing them from being implemented in industry. Prior research regarding this problem proposed using a LPF on the reset line. It proved to successfully reduce the excessive resets, but the phase margin was decreased as a side effect. Time regularization was also considered but it showed improvements only for a small frequency band.

This thesis proposed a solution that does not influence stability margins and improves the performance of reset control over a broad frequency range. The stability conditions for the control loops including the observer are derived by exploiting the H_β-condition. First, an architecture in which an observer was placed on the feedback line was shown to have good noise reduction possibilities. However, a major drawback was the dependence on an accurate model of the plant. Small deviations between plant and model were causing a large pseudo-sensitivity increase which verified similar conclusions from frequency domain formulas.

Therefore, a new control loop was presented in which a separate feedback line is created for the reset condition. Using an observer to estimate the plant state and filter out the measurement noise, the excessive resets were reduced. This led to less overshoot in the transient response of a CR-CgLp-PID controller. The pseudo-sensitivity for low frequencies was reduced with 11dB while the phase margin was not harmed. Besides this, the root mean square of the control output was reduced in the separate feedback architecture. When model inaccuracies of the plant model were studied, the phase difference caused by the observer was used to successfully approximate the pseudo-sensitivity. Good robustness to this modelling inaccuracies predicted by the analytical work was verified in numerical simulations. Concluding, by using an observer to filter out measurement noise, the transient and tracking performance of the CR-CgLp-PID controller was improved, therefore making reset control better implementable in practical setups.

8

Recommendations

The observer based filtering has proven to be a powerful tool to improve the performance of reset control when sensor noise is considered. This section discusses the thesis and gives recommendations for future research.

Extending the analytical work by including an analysis of the system in discrete time analysis might give insights in the implementation problems. Besides this, a method to combine the higher-order harmonics to generate a better approximation of the pseudo-sensitivity would be a large improvement on the method used in this thesis, since discrepancies between the analytical work and the simulations were seen.

Matching observer model with the plant can be difficult in practice. Right now, FRF fitting is still required if the observer is added to the system. In practice, the state space matrices have to be estimated based on FRF data of the plant. This data is commonly used for tuning already, but a fitting tool could be incorporated in the work to automate this process. Besides this, the tuning of the observer gain can be tedious for the same reason. In simulations, all noise parameters are known and therefore the covariance of the process and measurement noise can be used to calculate the optimal observer gain. A related matter is if the control system can become unstable by the mismatch between the plant and the observer model. The proof in section 6 suggests that this would not be the case, but further research could be done by studying delta matrices.

Non-zero-mean noise can be studied as a possible disturbance source. In practical, many noise sources can not be approximated by white noise. Quantization noise has been introduced quickly, but other, very low frequency noise sources such as thermal or fatigue effects are not considered in this thesis. Therefore these should be studied separately before implementing the architecture in high-tech systems.

Non-linear plants can be a weak spot of the presented architecture, since a model of the plant is required for the observer. Non-linear plant, or significant non-linear disturbances in the plant can potentially degrade the performance of the proposed control loop.

Bibliography

[1] R.H.M. Schmidt, G. Schitter, A. Rankers, and J. van Eijk. *The design of high performance mechatronics: high-tech functionality by multidisciplinary system integration*. IOS Press, Netherlands, 2nd revised edition, 2014.

[2] O. Beker, C.V. Hollot, and Y. Chait. Plant with integrator: an example of reset control overcoming limitations of linear feedback. *IEEE Transactions on Automatic Control*, 46(11):1797–1799, 2001.

[3] H. Nijmeijer L.Hazeleger, M. Heertjes. Second-order reset elements for stage control design. *Proceedings of the American Control Conference*, 2016-July:2643–2648, 7 2016.

[4] I. Horowitz and P. Rosenbaum. Non-linear design for cost of feedback reduction in systems with large parameter uncertainty. *International Journal of Control*, 21:977–1001, 1975.

[5] Y. Zheng, Y. Chait, C. V. Hollot, M. Steinbuch, and M. Norg. Experimental demonstration of reset control design. *Control Engineering Practice 8*, 1999.

[6] Y. Wang D. Wu, G. Guo. Reset integral-derivative control for hdd servo systems. *IEEE Transactions on Control Systems Technology*, 15:161–167, 1 2007.

[7] N. Saikumar, R. K. Sinha, and S. H. HosseinNia. 'constant in gain lead in phase' element-application in precision motion control. *IEEE/ASME Transactions on Mechatronics*, 24:1176–1185, 6 2019.

[8] A. A. Dastjerdi, N. Saikumar, and S. H. HosseinNia. Tuning of a class of reset elements using pseudo-sensitivities. In *European Control Conference (ECC)*, pages 1187–1192, 2021.

[9] N. Karbasizadeh and S. H. HosseinNia. Continuous reset element. *arXiv preprint arXiv:2110.12801*, 2021.

[10] C. Cai, A. A. Dastjerdi, N. Saikumar, and S.H. HosseinNia. The optimal sequence for reset controllers. *European Control Conference (ECC)*, 2020.

[11] A. A. Dastjerdi, A. Astolfi, N. Saikumar, N. Karbasizadeh, D. Valerio, and S H. HosseinNia. Closed-loop frequency analysis of reset control systems. *IEEE transactions on automatic control*, in press.

[12] K. J. Astrom. Limitations on control system performance. *European Journal of Control*, 6:2–20, 2000.

[13] A. Banos and A. Barreiro. *Reset control systems*. Springer, 2013.

[14] R. Miklosovic, A. Radke, and Z. Gao. Discrete implementation and generalization of the extended state observer. *Proceedings of the American Control Conference*, 2006:2209–2214, 2006.

[15] D. Yoo, S. S.T. Yau, and Z. Gao. Optimal fast tracking observer bandwidth of the linear extended state observer. *International Journal of Control*, 80:102–111, 1 2007.

[16] Y.-D. Yoon, E. Jung, A. Yoo, and S.-K. Sul. Dual observers for the disturbance rejection of a motion control system. *IEEE Industry Applications Annual Meeting*, 2007.

[17] J. Farrell. *4 State Estimation*. Academic press, 2005.

[18] H. Li, C. Du, and Y. Wang. Optimal reset control for a dual-stage actuator system in hdds. *IEEE/ASME Transactions on Mechatronics*, 16:480–488, 6 2011.

[19] R. E. Kalman. A new approach to linear filtering and prediction problems. *ASME - Journal of Basic Engineering*, 82:35–45, 1960.

[20] D. G. Luenberger. Observing the state of a linear system. *IEEE Transactions on Military Electronics*, 8:74–80, 1964.

[21] G. Bishop G. Welch. An introduction to the kalman filter. 1997.

[22] H. W. Sorenson. Least-squares estimation: from gauss to kalman. *IEEE Spectrum*, 7:63–68, 1970.

[23] J. Zheng, Y. Guo, M. Fu, Y. Wang, and L. Xie. Improved reset control design for a pzt positioning stage. 2007.

[24] N. Karbasizadeh, A. A. Dastjerdi, N. Saikumar, D. Valerio, and S. H. HosseinNia. Benefiting from linear behaviour of a nonlinear reset-based element at certain frequencies. *2020 Australian and New Zealand Control Conference, ANZCC 2020*, pages 226–231, 11 2020.

[25] Y. Guo, L. Xie, and Y. Wang. *Analysis and Design of Reset Control Systems*. Institution of Engineering and Technology, 11 2015.

[26] N. Saikumar, K. Heinen, and S. H.. HosseinNia. Loop-shaping for reset control systems. *Control Engineering Practice*, 111:104808, 6 2021.

[27] E. Akyiiz, N. Saikumar, and S. H. HosseinNia. Reset control for vibration disturbance rejection. *IFAC-PapersOnLine*, 52:525–530, 9 2019.

[28] M. S. Bahnamiri, N. Karbasizadeh, A. A. Dastjerdi, N. Saikumar, and S. H. HosseinNia. Tuning of cglp based reset controllers: Application in precision positioning systems. *IFAC-PapersOnLine*, 53:8997–9004, 2020.

[29] J. C. Clegg. A nonlinear integrator for servomechanisms. *Transactions of the American Institute of Electrical Engineers, Part II: Applications and Industry*, 77:41–42, 7 1958.

[30] A. Banos and A. Vidal. Definition and tuning of a pi+ci reset controller. *2007 European Control Conference, ECC 2007*, pages 4792–4798, 2007.

[31] X. Hou, A. A. Dastjerdi, N. Saikumar, and S. H. HosseinNia. Tuning of 'constant in gain lead in phase (cglp)' reset controller using higher-order sinusoidal input describing function (hosidf). *2020 Australian and New Zealand Control Conference, ANZCC 2020*, pages 91–96, 11 2020.

[32] H. Hu, Y. Zheng, Y. Chait, and C.V. Hollot. On the zero-input stability of control systems with clegg integrators. In *Proceedings of the 1997 American Control Conference (Cat. No.97CH36041)*, volume 1, pages 408–410 vol.1, 1997.

[33] O. Beker, C. V. Hollot, Y. Chait, and H. Han. Fundamental properties of reset control systems. *Automatica*, 40:905–915, 2004.

[34] A. Baños, J. Carrasco, and A. Barreiro. Reset times-dependent stability of reset control systems. *IEEE Transactions on Automatic Control*, 56:217–223, 1 2011.

[35] S. J.L.M. van Loon, K. G.J. Gruntjens, M. F. Heertjes, N. van de Wouw, and W. P.M.H. Heemels. Frequency-domain tools for stability analysis of reset control systems. *Automatica*, 82:101–108, 8 2017.

[36] A. A. Dastjerdi, A. Astolfi, and S. H. HosseinNia. Frequency-domain stability methods for reset control systems. *2020 59th IEEE Conference on Decision and Control (CDC)*, pages 5785–5791, 2020.

[37] J. Zheng and M. Fu. A reset state estimator using an accelerometer for enhanced motion control with sensor quantization. *IEEE Transactions on Control Systems Technology*, 18:79–90, 1 2010.

[38] B. Widrow, I. Kollar, and M.-C. Liu. Statistical theory of quantization. *IEEE Transactions on instrumentation and measurement*, 45:353–361, 4 1996.

[39] B. Kieft, S. H. HosseinNia, and N. Saikumar. Time regularization as a solution to mitigate quantization induced performance degradation. In *2021 European Control Conference (ECC)*, pages 2458–2464, 2021.

A

Model parameters

A.1. Model Parameters

The model parameters that were used are listed below. If not specified in the report specifically, these parameters were used.

Parameter	Value	Unit
ω_{BW}	942	rad/s
ω_r	172	rad/s
ω_{ra}	160	rad/s
ω_f	9420	rad/s
γ	0.5	-
ω_l	72.5	rad/s
ω_h	4710	rad/s
P	$5.3335 * 10^5$	-
ω_i	94.2	rad/s
ω_d	529.2	rad/s
ω_t	1678	rad/s
M	1	kg
f_s	10^4	Hz
Solver	ode1	-
A_{ref}	300	μm
A_n	3	μm
ω_n	102	rad/s
n	100	-
f_{ref}	$1 - 10^4$	Hz
Δ	9.8	μm
P_n	$2e^{-16}$	W

Table A.1: Numerical simulation parameters

A.2. Simulink model

The numerical simulations were done in Matlab/Simulink. The ”real-time” model was built in Simulink and the initialization and data acquisition was done in Matlab. An example control loop is given in Fig. A.1. The details on the construction of the CgLp element can be seen in Fig. A.2. A state space implementation of the full CgLp element was used; no separation was done in a FORE and linear lead element. A close up of the Kalman filter implementation is given in Fig. A.3.

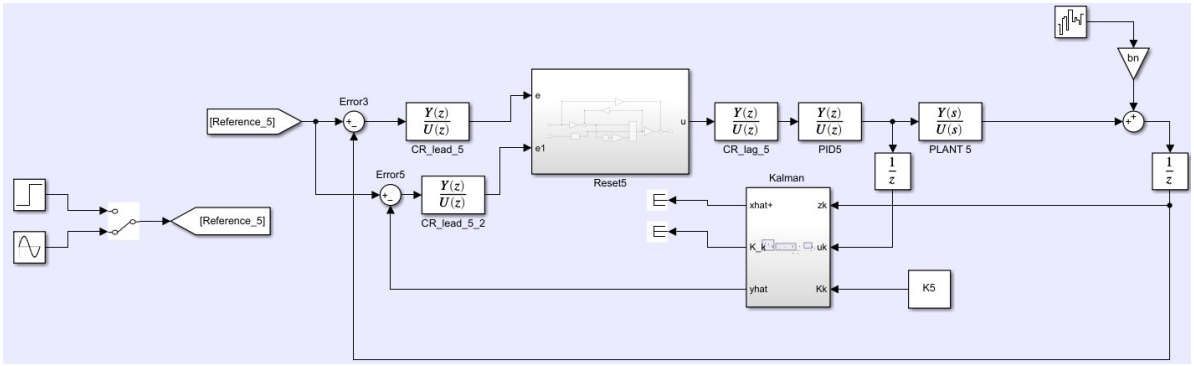

Figure A.1: Example of a control loop that was used for the numerical simulations in Simulink

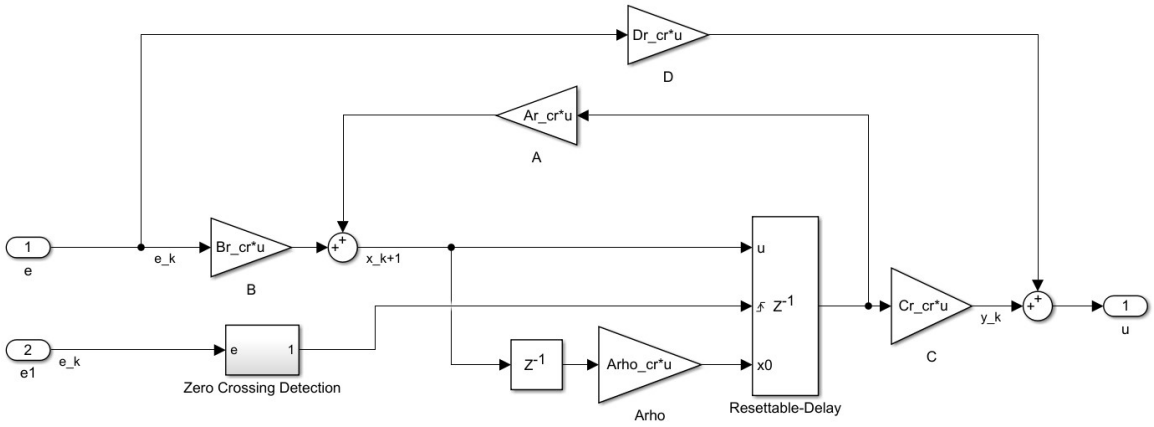

Figure A.2: Example of the CgLp element that was used for the numerical simulations in Simulink

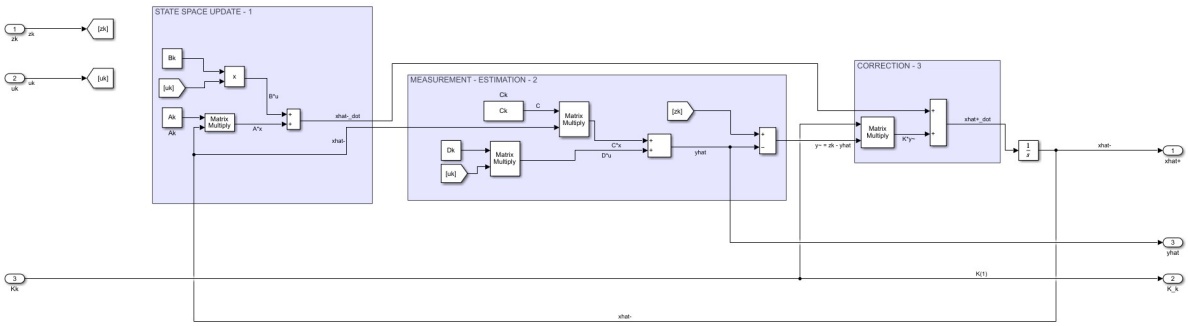

Figure A.3: Example of the static Kalman filter that was used for the numerical simulations in Simulink

B

Closed loop matrices

The matrix details of (5.1) are presented here. Let the system be separated in six different state space matrices: lead, CgLp, lag, PID, plant, and Kalman filter. Let the state space matrices be denoted by L, r, R, c, p, k respectively.

$$x(t) = \begin{bmatrix} x_L' & x_r' & x_R' & x_c' & x_p' & x_k' \end{bmatrix}' \tag{B.1}$$

The overall state space matrices then are:

$$\bar{A} = \begin{bmatrix} A_L & 0_{n_L \times n_r} & 0_{n_L \times n_R} & 0_{n_L \times n_c} & 0_{n_L \times n_p} & -B_L C_k \\ B_r C_L & A_r & 0_{n_r \times n_R} & 0_{n_r \times n_c} & 0_{n_r \times n_p} & -B_r D_L C_k \\ B_R D_r C_L & B_R C_r & A_R & 0_{n_R \times n_c} & 0_{n_R \times n_p} & -B_R D_r D_L C_k \\ B_c D_R D_r C_L & B_c D_R C_r & B_c C_R & A_c & 0_{n_c \times n_p} & -B_c D_R D_r D_L C_k \\ B_p D_c D_R D_r C_L & B_p D_c D_R C_r & B_p D_c C_R & B_p C_c & A_p & -B_p D_c D_R D_r D_L C_k \\ B_k D_c D_R D_r C_L & B_k D_c D_R C_r & B_k D_c C_R & B_k C_c & L C_p & A_k - L C_k - B_k D_c D_R D_r D_L C_k \end{bmatrix} \tag{B.2}$$

$$\bar{B} = \begin{bmatrix} B_L & 0_{n_L \times 1} \\ B_r D_L & 0_{n_r \times 1} \\ B_R D_r D_L & 0_{n_R \times 1} \\ B_c D_R D_r D_L & 0_{n_c \times 1} \\ B_p D_c D_R D_r D_L & 0_{n_p \times 1} \\ B_k D_c D_R D_r D_L & 0_{n_k \times 1} \end{bmatrix} \tag{B.3}$$

$$\bar{C} = \begin{bmatrix} 0_{1 \times n_L} & 0_{1 \times n_r} & 0_{1 \times n_R} & 0_{1 \times n_c} & C_p & 0_{1 \times n_k} \end{bmatrix} \quad \bar{D} = \mathbf{0} \tag{B.4}$$

And for the reset condition:

$$\bar{C}_e = \begin{bmatrix} C_L & 0_{1 \times n_r} & 0_{1 \times n_R} & 0_{1 \times n_c} & 0_{1 \times n_p} & -D_L C_k \end{bmatrix} \tag{B.5}$$

$$\bar{D}_e = \begin{bmatrix} D_L & 0 \end{bmatrix} \tag{B.6}$$

C

Transfer functions in DT

The continuous time transfer functions of the control loop that were used in the thesis can also be derived in discrete time. This process was not finished since it is not considered to be a critical aspect, but can be useful in future research. A start is made below. Note that the state space matrices and the observer gain vector are not equal to their continuous time equivalent that is used in the continuous time case in the thesis.

The plant process is modeled as (C.1) and (C.2) .

$$x_k = A_p x_{k-1} + B_p u_{k-1} \tag{C.1}$$

$$y_k = C_p x_k + D_p u_k \tag{C.2}$$

The measurement of the plant output is modeled.

$$z_k = C_p x_k + w_k \tag{C.3}$$

Where we again assume that the noise is Gaussian distributed with zero mean. The discrete time observer equations can be seen in (C.4) and (C.5).

$$\hat{x}_k = A_L \hat{x}_{k-1} + B_L u_{k-1} + L(z_k - \hat{y}) \tag{C.4}$$

$$\hat{y}_k = C_L \hat{x}_{k-1} + D_L u_{k-1} \tag{C.5}$$

After substitution, we come to (C.6).

$$\hat{x}_k = A_L \hat{x}_{k-1} + B_L u_{k-1} + L\left(C_p x_{k-1} + D_p u_{k-1} + w_{k-1} - C_L \hat{x}_{k-1} - D_L u_{k-1}\right) \tag{C.6}$$

$$\hat{x}_k = (A_L - LC_L)\hat{x}_{k-1} + (B_L - LD_L)u_{k-1} + LC_p x_{k-1} + LD_p u_{k-1} + Lw_{k-1} \tag{C.7}$$

We start with calculating the plant state x_k by summing over all the previous steps.

$$x_k = A_p^k x_0 + \sum_{n=1}^{k} A_p^{n-1} B_p u_{k-n} \tag{C.8}$$

Eq. (C.8) can be substituted in (C.7), with plant state $k-1$

$$\hat{x}_k = (A_L - LC_L)\hat{x}_{k-1} + (B_L - LD_L + LD_p)u_{k-1} + LC_p\left(A_p^{k-1} x_0 + \sum_{n=1}^{k-1} A_p^{n-1} B_p u_{k-1-n}\right) + Lw_{k-1} \tag{C.9}$$

And in order to directly calculate the desired $\hat{x}$, one can write the sum over all the previous time steps.

$$\hat{x}_k = (A_k - LC_k)^k \hat{x}_0 + \sum_{m=1}^{k} (A_k - LC_k)^{m-1}\left[(B_k + LD_p - LD_k)u_{k-m} + \left(A_p^{k-m} x_0 + \sum_{n=1}^{k-m} (A_p^{n-1} B_p u_{k-n-m}\right)\right] \tag{C.10}$$

D

Estimating phase delay

D.1. Predicting the phase delay of a Kalman filter

Some effort was put into the estimation of the phase delay of a Kalman filter. A LPF is able to filter out the noise and therefore improve the zero-crossing detection, but it comes at the cost of a phase delay that (partly) removes the benefit of the non-linear CgLp controller. Therefore, the phase delay of the Kalman filter was identified as an critical topic of research. It could be a potential downside of the proposed methods.

To calculate the phase delay, a numerical approach was used to approximate the DF of the filter. Since the Kalman filter is a Multi Input Single Output (MISO) system, it was analysed together with the plant and sensor to get a Single Input Single Output (SISO) system. Figure D.1 shows a schematic of the analysed system. Another argument to extend the scope of this analysis is that a Kalman filter is not a frequency filter and is therefor probably not very well captured in frequency domain on its own. However, when including the plant and sensor, the Kalman filter could be interesting to study.

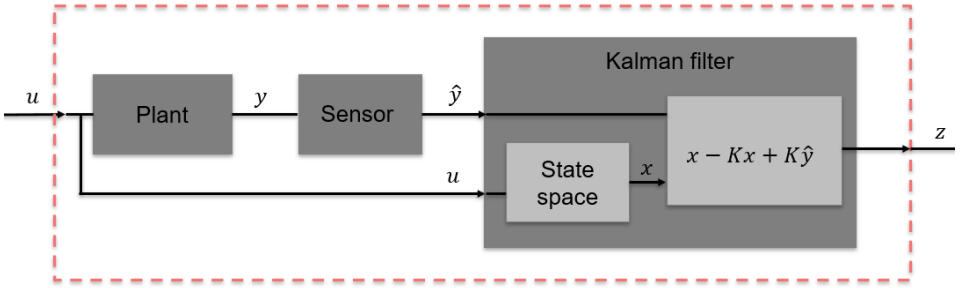

Figure D.1: SISO system: a plant, sensor, and Kalman filter

The first order harmonic is described by the first order Fourier series of the output, when a sinusoidal input is given:

$$x(t) = Xsin(\omega t), y(t) = A_1 cos(\omega t) + B_1 sin(\omega t) \tag{D.1}$$

The describing function for that specific frequency ω can then be calculated as:

$$|DF(\omega)| = \frac{\sqrt{A_1^2 + B_1^2}}{X}, \angle DF(\omega) = tan^{-1}(\frac{B_1}{A_1}) \tag{D.2}$$

The coefficients A_1 and B_1 can be calculated with the Fourier integral:

$$A_1 = \frac{1}{\pi}\int_0^{2\pi} y(t)cos(\omega t)\, d(\omega t) \tag{D.3}$$

$$B_1 = \frac{1}{\pi}\int_0^{2\pi} y(t)sin(\omega t)\, d(\omega t) \tag{D.4}$$

As a first try, the sensor was assumed to be ideal. The output of the Kalman filter is therefor perfectly resembling the model of the mass plan. The result can be seen in Figure D.2. The result does not satisfy, since the data around the bandwidth does not look very trustworthy.

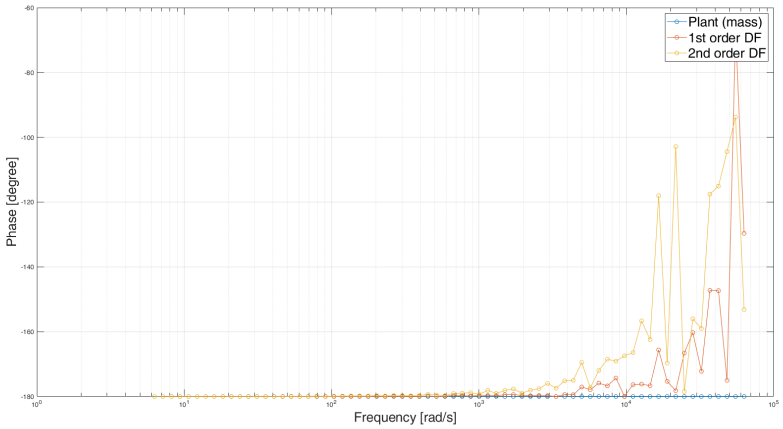

Figure D.2: Phase plot of the first and second order DF, numerically approximated

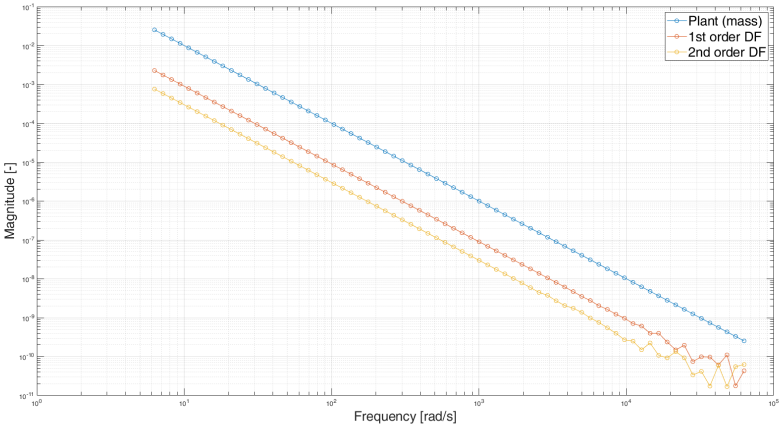

Figure D.3: Magnitude plot of the first and second order DF, numerically approximated

Depending on the sampling rate, since that is also determining the process speed of the Kalman filter, the linearizer tool from Matlab results in Figure D.4.

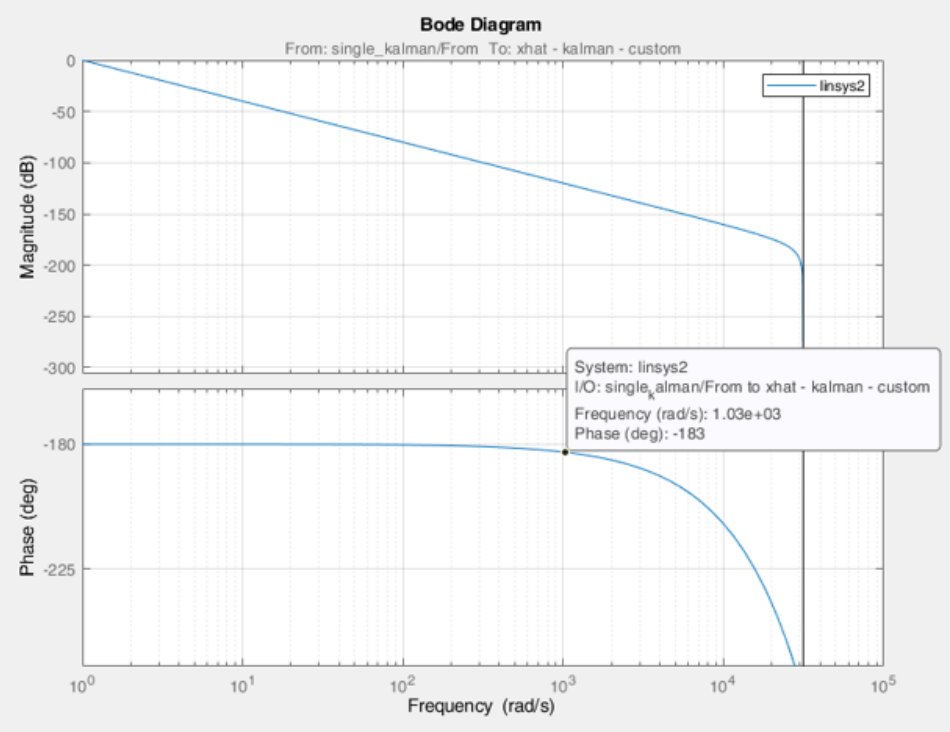

Figure D.4: First order DF found by Simulink linearizer tool